Civil Engineering ETDs

Engineering ETDs

7-11-2013

Reconsidering Composite Action on Strength of Wood Roof Systems

Ivan Antonio CamposVarela

Follow this and additional works at: https://digitalrepository.unm.edu/ce_etds

IVAN ANTONIO CAMPOS VARELA
Candidate

CIVIL ENGINEERING
Department

This thesis is approved, and it is acceptable in quality and form for publication:

Approved by the Thesis Committee:

Walter Gerstle , Chairperson

Arup Maji

Timothy Ross

Stephen Dwyer

RECONSIDERING COMPOSITE ACTION ON STRENGTH
OF WOOD ROOF SYSTEMS

by

IVAN ANTONIO CAMPOS VARELA

B.S. CIVIL ENGINEERING
UNIVERSITY OF CHIHUAHUA, 2010

THESIS

Submitted in Partial Fulfillment of the
Requirements for the Degree of

Master of Science

Civil Engineering

The University of New Mexico
Albuquerque, New Mexico

May, 2013

RECONSIDERING COMPOSITE ACTION ON STRENGTH

OF WOOD ROOF SYSTEMS

By

Ivan Antonio Campos Varela

B.S., Civil Engineering, University of Chihuahua, 2010

M.S., Civil Engineering, University of New Mexico, 2013

ABSTRACT

Structural aspects of the installation of photovoltaic (PV) modules on existing wood roof framing systems are considered. Often, existing roofs are inadequate to resist even current minimum design loads, much less the extra weight of PV modules. Rather than requiring expensive retrofits, it is desired to bring these under-strength roofs into compliance with current codes by reconsidering composite action, produced by the joist-sheathing interaction of the assembly, on the bending strength of joists.

The effect of composite action can be quantified by considering a composite T-beam, with the wood joist being the web and the structural sheathing being the flange. Although this effect has already been considered in the past (under different assumptions and different models), it is hypothesized that an increase in strength can still be achieved even when using a discontinuous flange (due to gaps between sheathing panels), and non-rigid connections like a nailed joint.

Laboratory experiments using several 2"x 4" bare wood joists and 2"x4" joists along with 7/16"-thick OSB panels attached to their tops (using nailed and glued-and-

nailed connections) were performed. The experiments showed bending strength increases between 18 to 60% in T-beams, when compared to the bending strength of bare joists. Tests also showed that the strength of the T-beam varies as a function of the random location, with respect to the location of a gap, of a weak knot with lower strength that initiates failure in the joist. The behavior and mechanical properties of the connection are also studied and compared with existing literature.

Analytical and finite element analyses of the composite T-beam subjected to constant moment, show nonlinear behavior of the nailed connection when the failure moment is applied to the composite T-beam, hence, developing Nonlinear Partial Composite Action (NPCA). A small decrease in the maximum tensile stress at the bottom of the joist is obtained at sections away from the location of the gap due to NPCA. Also, finite element analysis shows that even at the location of the gap, the tensile stress is slightly reduced due to local effects in the joist produced by the local nail forces.

A Monte Carlo simulation is utilized to randomly vary the location of knots along the span of the T-beam and conservatively evaluate the effect that NPCA has in the tensile stress at each knot. Slight increases in the mean bending strength of the joist are predicted, depending upon the 5% exclusion limit bending strength value for clear wood and the stress grade of the species. However, these predictions of strength increase are small and do not match the 18 to 60% observed increases in the laboratory experiments. Perhaps the number of laboratory tests was insufficient to produce a statistically significant data set.

Finally, generic, easy to install and effective procedures for retrofitting roof joists to enhance the beneficial effects of NPCA are proposed to justify increased roof strength to allow for the loads from the PV modules.

DEDICATION

To my parents and fiancée…

ACKNOWLEDGMENTS

TABLE OF CONTENTS:

List of Figures

x

List of Tables

Chapter 1   Introduction

1.1 Motivation

Recently, many home-owners have attempted to install solar photovoltaic (PV) modules on their existing roof systems, as shown in Fig. 1.2, but many have been unable to obtain engineering certification because of the extra weight of the PV modules and because often the roof's calculated load-carrying capacity is even inadequate to resist current minimum design loads specified by local building codes. There are many reasons why the roofs do not meet modern structural codes such as ASCE 7-10 [ASCE 2010]: modern design wind and snow loads are greater than in earlier codes, many houses were not originally designed by engineers, and design codes such as the National Design Specification [NDS 2005] strength specifications have changed over the years. Nonetheless, failures of wood roof systems subjected to design loads have been extremely rare and, apparently no failures have been reported due only to addition of the solar PV modules, which in some cases, even improve safety because the most severe wind loads on roofs are typically of an uplift nature.

Figure 1.1 PV modules on roof framing systems.

1.2 Background

Light-frame wood structural systems have been used for many years in residential construction in the United States. These framing systems consist of wall, floor, and roof systems, and are generally composed of repetitive members, like solid-sawn wood joists or trusses, in combination with structural sheathing like plywood or Oriented Strand Board (OSB). This research focuses just on the strength of roof framing systems.

A typical residential roof framing system is composed of visually graded wood joists or prefabricated wood trusses at 24" spacing, with plywood or OSB sheathing nailed to the top of the joists at 12" spacing. The structural sheathing is usually fabricated in 4'x 8' panels, with a 1/8" gap between them to account for linear expansion effects, as shown in Fig. 1.1.
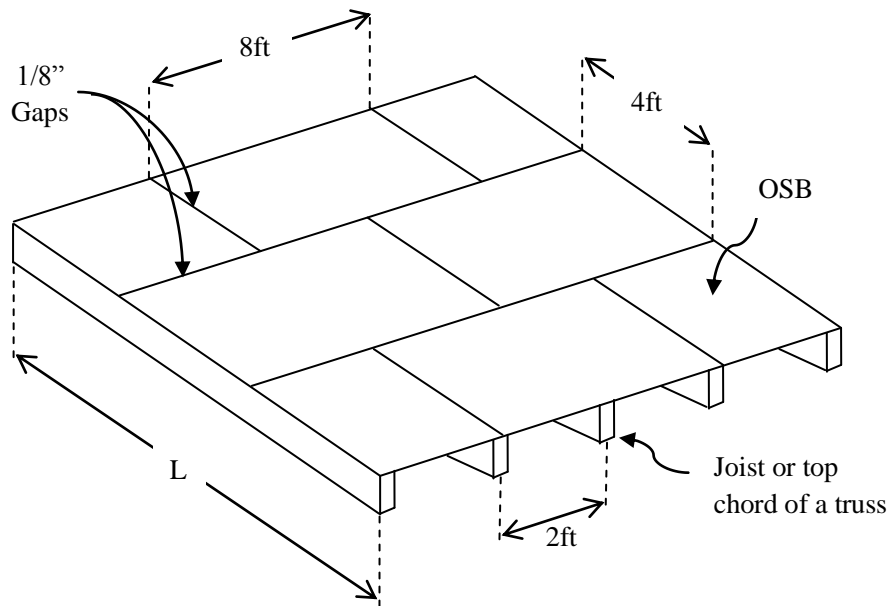
Figure 1.2 Typical roof system in residential housing.

Current engineering practice calculates the roof's load carrying capacity based upon conservative procedures that analyze the behavior of a single independent joist with several factors of safety (like assuming the most severe strength reducing characteristics and the 5% exclusion limit for clear wood strength values for each group species), instead of considering the joist-sheathing assembly to be acting as a whole, indeterminate system

2

that could produce a higher strength, that would be capable of resisting the updated minimum design loads and the extra weight of PV modules.

Some system effects are conservatively taken into account by the NDS design code [NDS 2005] when calculating the bending strength of a wood joist that is part of a redundant joist-sheathing system. A 15% increase of the allowable bending properties of the joists was established in the code, which considers load sharing and composite action effects. However, it is believed that the composite action effect should be reconsidered because of the assumptions made to obtain this increase, which will be explained and criticized in subsequent chapters.

1.3 Scope of work

There are many other system effects that may be considered when analyzing the roof framing systems to justify a higher bending strength, but this research focuses only on the interaction between the joist, the non-rigid connection provided by the nails, the discontinuous structural sheathing, and the effects this composite behavior may have on the strength of roofs. This research also focuses on developing generic, efficient and safe retrofits that would allow faster engineering approval for PV module installation.

1.4 Objectives

Rather than requiring expensive retrofits to existing roofs that do not satisfy the current codes and provisions, so that they can resist the extra weight of the unballasted PV modules (estimated to weigh less than 5 psf), it is desirable to investigate in more detail the actual (as opposed to code-predicted) strength of the existing roofs. The purpose of this research is to determine by testing and calculation if there is an increase in the bending strength of the wood joists by considering composite behavior, even when gaps in the sheathing are present.

It is hypothesized that the actual strength of roofs might be at least statistically higher than traditional methods of analysis would predict. If so, this additional strength could justify the additional loads of PV modules. If the roofs are still not strong enough,

3

then the objective is to produce a set of recommended retrofitting techniques for existing roofs. If this is successfully achieved, then the barrier to the installation of PV modules would be powered, by reducing the time necessary to get engineering approval for the installation, thus aiding the growth of the solar energy industry.

1.5 Thesis outline

Chapter 2 is a summary of the analyses and methods previously developed that considered different system effects on wall, floor and roof systems, and an explanation of why they do not satisfy the stated problem. The procedures and results from the laboratory experiments that were conducted throughout this research are fully described in Chapter 3. Chapter 4 describes the analytical and numerical analyses of the laboratory tests that were conducted in an effort to understand the mechanical behavior of the composite beam. The proposed statistical model and its assumptions to justify an increase in the statistical bending strength of the composite wood joists are explained in Chapter 5. Some retrofitting techniques are proposed in Chapter 6, based on the results of this research. Finally, Chapter 7 presents a summary, conclusions, and recommends future work.

Chapter 2   Literature Review

2.1 Introduction

Previous researchers have studied the interaction between wood joists/trusses and structural sheathing used for roof and floor assemblies. They have studied system effects like composite action, load sharing, and stiffness variability, among others, many of which have been recognized to improve the overall performance of the assemblies. This research is focused on just one of these effects: composite action.

Full Composite Action (FCA) cannot be achieved between the sheathing and the joist because of the non-rigidity of their connection (glue, nails, or both) and the presence of gaps in the sheathing, developing only "Partial Composite Action" (PCA). The shear force, F, generated at the interface between the sheathing and the joist is determined by the load-displacement curve (shown in Fig. 2.1) of the connectors and the magnitude of the differential lateral displacement (interlayer slip), δ, between these two members of the composite section. If the forces being carried by the connectors are below their yield strength (linear elastic region in Fig. 2.1), then the behavior of the interface will be linear and "Linear Partial Composite Action" (LPCA) will be developed; if these forces in the connectors are higher than the yield strength (nonlinear region), then the behavior of the interface will be nonlinear and "Nonlinear Partial Composite Action" (NPCA) will be developed.
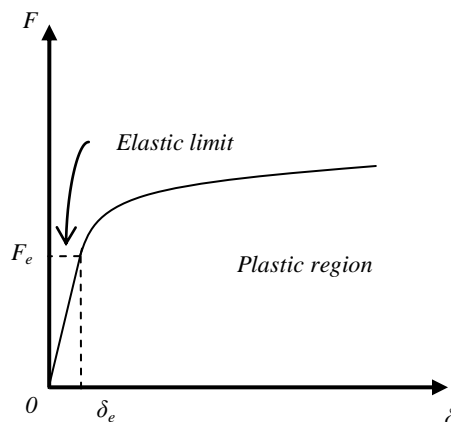
Figure 2.1 Typical load-displacement curve a nail.

2.2 Composite action and system effects

Kuenzi and Wilkinson [Kuenzi and Wilkinson 1971], developed deflection and maximum stress equations for two specific loading conditions: four point bending, as shown in Fig 2.2, and distributed load for simply-supported beams with continuous sheathing and LPCA.
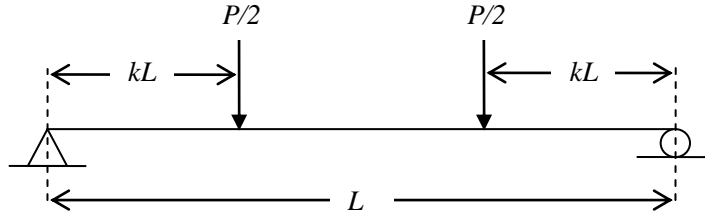
Figure 2.2 Definition of geometric parameters of the composite beam.

According to Kuenzi and Wilkinson [Kuenzi and Wilkinson 1971], the midspan deflection for four point bending, Δ, is given by

$$\Delta = \frac{k\left(3-4k^2\right)PL^3}{48(EI)_R}\left\{1 + \frac{6}{(3-4k^2)}\left[\frac{(EI)_R}{(EI)_u} - 1\right]\left(\frac{2}{\alpha L}\right)^2\left(1 - \frac{\sinh\alpha kL}{\alpha kL\cosh\frac{\alpha L}{2}}\right)\right\} , \qquad (2.1)$$

where

P is the applied load,

L is the span length,

k defines load position (shown in Fig. 2.2.),

$(EI)_R$ is the stiffness of the T-beam assuming full composite action,

$(EI)_u$ = stiffness of all beam components as if unconnected,

$$\alpha^2 = \frac{h^2 S}{(EI)_R - (EI)_u}\left[\frac{(EI)_R}{(EI)_u}\right], \qquad (2.2)$$

h is the distance between the centroid of the joist and centroid of the sheathing, and

6

S is the shear force, F, per unit nail spacing, s, per unit slip, δ, between principal members given by

$$S = \frac{F/\delta}{s} \ . \tag{2.3}$$

Kuenzi and Wilkinson [Kuenzi and Wilkinson 1971] also derived equations for maximum tensile and compressive stresses of the composite section for the same two loading conditions. However, these equations are not applicable when calculating the bending strength of the composite T-beam because of the assumption of continuous sheathing and LPCA, and because some parameters in the equations were not clearly defined.

A method to estimate the linear interlayer stiffness value was also developed by Wilkinson, where he took into account the properties of the nails like diameter, bending stiffness, and length (note that the yield strength of the nails was not considered), and the properties of the different materials in the assembly [Wilkinson 1972, 1974]. Unreasonably, this interlayer stiffness was assumed to remain linear elastic even when the equations were utilized to calculate the bending strength of the composite beams based on experimental failure loads.

McCutcheon modified the deflection equations of Kuenzi and Wilkinson [Kuenzi and Wilkinson 1971] and developed a method for predicting the stiffness of wood-joist floor systems with partial composite action, with a layer of sheathing on only one side of the joist [McCutcheon 1977] and on both sides of the joist [McCutcheon 1986].

Rearranging terms in Eq. (2.1)

$$\Delta = \frac{k(3-4k^2)PL^3}{48(EI)_R}\left\{1 + \left[\frac{6}{(3-4k^2)}\left(\frac{2}{\alpha L}\right)^2\left(1 - \frac{sinh\,\alpha kL}{\alpha kL\,cosh\frac{\alpha L}{2}}\right)\right]\left[\frac{(EI)_R}{(EI)_u} - 1\right]\right\}, \tag{2.4}$$

and replacing the term in the first square brackets by the empirical formula:

$$f_\Delta = \frac{10}{(L_f\alpha)^2+10} \tag{2.5}$$

7

where L_f is the distance between gaps in the sheathing, and α is defined by Eq. (2.2).

now Eq. (2.4) becomes:

$$\Delta = \frac{k(3-4k^2)PL^3}{48(EI)_R}\left[1 + f_\Delta\left(\frac{(EI)_R}{(EI)_u} - 1\right)\right]. \tag{2.6}$$

McCutcheon [McCutcheon 1977, 1986] also defined the effective stiffness of the partial composite section (to be utilized in the elementary beam deflection formulas) for T-beams as

$$EI = (EI)_u + \frac{\overline{(EA_f)}(EA_w)}{\overline{(EA_f)}+(EA_w)}\,h^2\ , \tag{2.7}$$

$$\overline{EA_f} = \frac{EA_f}{1+10\frac{EA_f}{SL_f^2}}\ , \tag{2.8}$$

where

EA_f is the axial stiffness of the flange,

EA_w is the axial stiffness of the web, and

$\overline{EA_f}$ is the reduced axial stiffness of the flange.

These T-beam and I-beam models continued to assume LPCA, but now they also considered the effects of discontinuities in the sheathing along the span of the joists due to gaps between the panels, and estimated the interlayer slip of the connection when calculating this effective stiffness.

McCutcheon's analytical method [McCutcheon 1977] was utilized in further research by R.W. Wolfe [Wolfe 1990], with defined values of interlayer stiffness based on some APA recommendations (only for glued-and-nailed and glued tongue & groove connections) mainly to calculate the increase in stiffness of the composite section, although the method was also utilized to calculate an increase in strength. Unreasonably, this increase in strength was calculated as the ratio of an effective section modulus (from McCutcheon's T-beam model [McCutcheon 1977]) to the section modulus of a bare joist.

8

Results were presented for glued-and-nailed joists only, while only-nailed joists calculations were not performed because they were said to produce no increase in strength due to inconsistencies in experimental results of some assemblies. Nevertheless, a glued-and-nailed connection is not commonly utilized in roof assemblies and can be highly inefficient and expensive as a possible retrofit to account for extra loads of solar panels. Thus, Wolfe's methods were not adopted.

Wolfe [Wolfe, R. W. and LaBissoniere, T. 1991] also tested three roof assemblies with two different truss configurations (Fink and scissors). He concluded that at failure loads, the nailed connections between the sheathing and the top-chord of the trusses were stressed beyond the elastic limit, and he said that NPCA has little effect on reducing the tensile stresses of the top-chord due to bending moments and thus, composite action should be ignored. This conclusion is premature, and it is reconsidered in this thesis.

Other system effects of roof assemblies like "load sharing" or "two-way action" have also been investigated over the years. Many researchers [Thompson, Vanderbilt, Goodman 1977; Foschi 1982; Wheat, Vanderbilt, and Goodman, 1983; Wolfe 1990; Wolfe and LaBissoniere 1991; Wolfe, and McCarthy 1989; McCutcheon 1984; Liu and Bulleit 1995; Cramer, Drozdek, and Wolfe 2000; Cramer, and Wolfe 1989; Rosowsky, Yu 2004; and Yu 2003] have developed a variety of analytic and numeric methods to try to account for these effects when calculating the strength and stiffness of the assembly. Also, some other researchers [Limkatanyoo 2004; Gupta, Miller, and Dung 2004] have focused on analyzing the roof as a whole and complex system, taking into consideration other effects. Limkatanyoo [Limkatanyoo 2004] included system effects in three-dimensional roof assemblies like the "reduced applied load effect", the "truss-to-truss support effect" and the "stiff-truss effect". He also performed a parametric study with the LPCA T-beam model developed by McCutcheon but he only found a 3% to 5% increase in the stiffness of the truss, so he ignored this composite action effect.

Several computer programs have also been developed to take into account these system effects for floors and framing walls: linear analysis programs like FEAFLO (Finite Element Analysis of Floors) by Thompson [Thompson et al. 1977], FAP (Floors

9

Analysis Program) by Foschi [Foschi 1982], FINWALL, by Polensek [Polensek 1976], and non-linear analysis programs like NONFLO (Nonlinear Floors) by Wheat [Wheat 1983], and BSAF (Beam-Spring Analog for Floors) by Liu and Bulleit [Liu and Bulleit 1995]. Although the engineering community recognizes the existence of these additional system effects, they are not the main topic of this research.

As a result of load sharing, the repetitive member factor (C_r) was established by the National Design Standards (NDS) [NDS 2005] and permits a 15% increase in the allowable joist bending stress value for the ASD method and a factor of 1.15 for the nominal strength value for the LRFD method, when the roof of floor assemblies meet certain requirements [NDS Section 4.3.9] It is important to note that this 15% increase in the allowable bending stresses ignores effects like gluing the joists to the sheathing or a closer spacing between joists, which would produce a higher strength for the assembly.

Application	Recommended C_r Value	References
Two adjacent members sharing load	1.1 to 1.2	AF&PA, 1996b HUD, 1999
Three adjacent members sharing load	1.2 to 1.3	ASAE, 1997
Four or more adjacent members sharing load	1.15	NDS
Wall framing (studs) of three or more members spaced not more than 24 inches on center with minimum 3/8 inch-thick wood structural panel sheathing on one side and ½ inch-thick gypsum board on the other side	1.5 – 2x4 or smaller 1.35 – 2x6 1.25 – 2x8 1.2 – 2x10	AF&PA, 1996b SBCCI, 1999 Polensek, 1975

Table 2.1 Recommended repetitive member factors for dimension lumber used in framing systems [Residential Structural Design Guide: 2000 edition].

Also, increases of up to a 50% in the bending strength of wall framing studs have been established due to system effects and composite action as shown in Table 2.1, based

on previous research by Polensek [Polensek 1976] and Douglas and Line [Douglas and Line 1996]. However, these factors have not been recognized yet by the NDS, and the increases where composite action is taken into account are only for wall studs with two layers of sheathing with specific characteristics and not for roof joists or trusses.

Rosowsky and Yu [D.V. Rosowsky and G. Yu 2004] developed another approach for wall framing, although it may be suitable also to any system composed of repetitive members. They proposed a "partial system factor approach for repetitive members", which considers a different factor for each of the system effects they studied (LPCA, system size, postyield behavior, and load sharing), instead of having just one single factor like the 1.15 given by the NDS to account for all of them together.

The proposed factor by Rosowsky and Yu for partial composite action was calculated as the ratio of the maximum bending stress of the bare joist to the maximum bending stress of the composite section:

$$K_{PCA} = \frac{\sigma_{bare}}{\sigma_{PCA}}, \tag{2.9}$$

where σ_{PCA} is derived as follows.

The total resisting moment, M_{Tot}, of the composite section shown in Fig. 2.3 is given by

$$M_{Tot} = M_j + M_s + Qh, \tag{2.10}$$
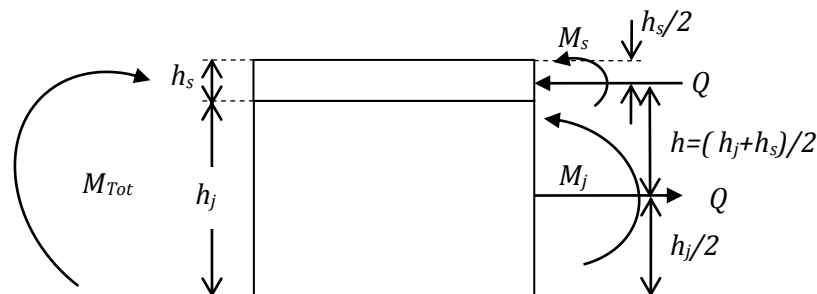
Figure 2.3 Rosowsky and Yu T-beam model [Rosowsky and Yu 2004]

11

Assuming each layer is bent to the same radius of curvature

$$M_j = \frac{EI_j}{EI}\, M_{Tot} \ , \text{and} \tag{2.11}$$

$$M_s = \frac{EI_s}{EI} M_{Tot} \ , \tag{2.12}$$

where

EI_j is the bending stiffness of the joist,

EI_s is the bending stiffness of the sheathing, and

EI is the effective bending stiffness of the LPCA (using McCutcheon's method).

Substituting Eqs. (2.11) and (2.12) into eq. (2.10) and solving for Q

$$Q = \frac{M_{Tot}}{h}\left(1 - \frac{EI_s + EI_j}{EI}\right). \tag{2.13}$$

The maximum bending stress of the partial composite section, σ_{PCA}, is given by:

$$\sigma_{PCA} = \frac{Q}{A_j} + \frac{M_j}{S_j}, \tag{2.14}$$

where

A_j is the cross sectional area of the bare joist, and

S_j is the section modulus of the bare joist.

The maximum bending stress at the bottom of the bare joist, σ_{bare} is given by:

$$\sigma_{bare} = \frac{M_{Tot}}{S_{bare}}, \tag{2.15}$$

12

Eq. (2.16) is obtained by substituting Eqs. (2.11), (2.12), (2.13), (2.14), and (2.15) into Eq. (2.9):

$$K_{PCA} = \frac{6(EI)h}{6(EI_j)h + h_j[EI - (EI_j + EI_s)]},$$
(2.16)

where

h_j is the depth of the bare joist. As explained further below, this method cannot be correct because EI does not account for NPCA.

On the other hand, an approach to achieve FCA was utilized by Rancourt [Rancourt 2008] using wood I-joists/oriented strand board (OSB) roof panel assemblies. He utilized OSB sheathing on the top and bottom of the I-joist with glued joints, obtaining up to a 124% increase in strength and a 115% increase in stiffness compared to the bare I-joist. This was achieved using continuous OSB sheathing (up to 16 feet long), developing FCA of the panel. However, such an assumption cannot be made for typically-sheathed roof framing, in which the sheathing is typically nailed to the framing as explained earlier.

2.3 Conclusions

It is important to note that in all of the previous models where McCutcheon's approach [McCutcheon 1977] was utilized to calculate an increase in strength in the T-beam with LPCA, there are certain effects that are not considered in his analysis:

1. Nonlinear behavior of the nails. This behavior strongly affects the magnitude of the axial force being carried by the sheathing, as the axial force in the sheathing behaves nonlinearly after the nails have yielded, and hence, the maximum tensile stress at the bottom of the joist will also be affected.

2. Effect of gaps in sheathing on strength. Considering the assumptions Rosowsky and Yu made, the bottom tensile stresses are constant throughout the length of the joist and might be calculated as in Eq. (2.14) if the nails have not reached their nonlinear range

13

(LPCA). Recall that Eq. (2.14) is based on McCutcheon's approach, which only considers the effect of the gaps when calculating the effective bending stiffness of the composite section. If the nails have started yielding, then a new formulation is needed to take into account this behavior (NPCA). However, NPCA is developed only at sections away from a gap location. In sections close to a gap, the tensile stresses will increase, reaching a maximum value close to that of a bare joist at the location of the gap (as will be shown in this research), meaning that there is no overall increase in strength in the partial composite section if no other parameters are considered.

All of the previously described research focused mainly on calculating the stiffness of the composite section with LPCA, considering two-way action based on the stiffness variability of the members, analyzing load redistribution of a system once the first member fails, and analyzing the roof assembly as a complex 3-D system, but none mentioned the effects on the bending strength of an assembly with gaps in sheathing considering NPCA. It is hypothesized that a quantified increase in the nominal bending strength of traditionally-sheathed composite roof systems can be achieved even when considering a discontinuous flange. To test this hypothesis, laboratory experiments, and theoretical, numerical, and statistical analyses have been conducted in this thesis and are described in the following chapters.

Chapter 3   Experiments

3.1 Introduction

To test the hypothesis that there might be an increase in the bending strength of the wood joists because of the possible benefits of NPCA provided by the structural sheathing attached to the top of the joist (even when using traditional roof framing systems), a series of laboratory experiments were performed. Their procedures and results are presented next.

3.2 First set of experiments – roof assemblies

3.2.1   Test setup

Three dimension lumber and structural sheathing assemblies similar to those commonly utilized in roof systems of residential housing were loaded to failure in a four-point bending test. This loading configuration produces a constant moment and no shear forces between the two point loads, as shown in Fig. 3.1. Sufficient spans, a, were utilized to avoid a shear failure at the ends of the member before a bending failure occurs in the constant moment region.
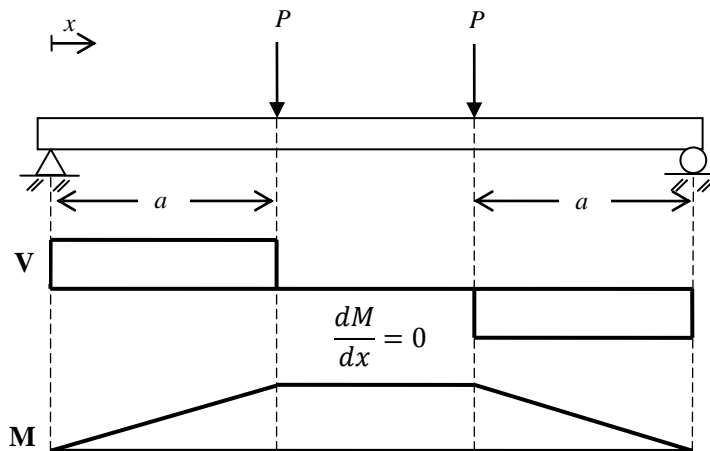
Figure 3.1 Bending moment and shear force diagrams for four-point bending test.

The first assembly consisted of three simply-supported 2"x 4"x 8' bare wood joists, spaced at 24". The joists were laterally braced, as shown in Fig. 3.2, to avoid any lateral torsional buckling effects. The second assembly consisted of the same 2"x 4"x 8'

15

wood joists spaced at 24", but in this test two 7/16"x 4'x 4' OSB panels were attached to the tops of the joists, leaving a 1/8" gap at midspan, as shown in Figs. 3.3 and 3.4. The OSB's strong axis was oriented perpendicular to the longitudinal axis of the joists. A nailed joint (8d nails at 12" spacing) was utilized to connect the OSB panels to the joist. The third assembly was the same as the second, but with a glued-and-nailed joint at the interface. The wood joists were selected from the same batch to permit evaluation of their bending strengths and stiffnesses when interacting with the OSB panels.

Figure 3.2 First test setup.

Figure 3.3 Second and third tests setup.

16

Figure 3.4 Gap at midspan in OSB sheathing.

The MTS hydraulic actuator model 244.23 from UNM's structures laboratory was utilized to test all the specimens. The idealization of each joist in the assembly is shown in Fig. 3.5. Load was applied using a W12x45 steel beam, which transferred the load applied by the actuator to two 2"x 12" wood joists spaced at 3', which transferred the loads to the assembly as two point loads (Figs. 3.2 and 3.3). Two Round HSS 4.5" x 3/8" were used as the supports; the first support was restrained against movement in the direction of the longitudinal axis of the joists (pinned support) while the second was able to roll in the same direction (roller support).
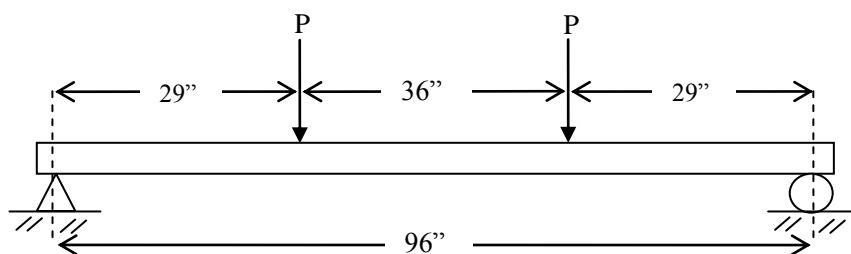
Figure 3.5 Idealization of supports and loading conditions.

3.2.2 Materials

Three 2"x 4" (nominal) x 8' long hem-fir joists visually graded as studs by the Western Wood Products Association (WWPA) and two 4'x 4' sheets of 7/16'' thick OSB were utilized per roof assembly. Also two 2" x 12" (nominal) wood joists (to transfer the

17

loads), a PL 400 Floor and Deck semi-structural adhesive (satisfies ASTM D3498 [ASTM, International 2005]), 8d-2 ½'' long common wire nails, and the MTS Hydraulic Actuator were utilized in the experiments.

3.2.3   Procedure

The actuator was controlled by a computer which, along with a data acquisition system, registered data points of load and displacement of the wide flange section. The load was applied using displacement control with a rate of 0.10 in/min, to avoid any dynamic effects on the sample. The assemblies were loaded to failure.

3.2.4   Results

The following results were obtained. The effects of self-weight of the members were neglected because of their low values (26 lb per point load and 4.63 lb/ft for the 8' long joist and OSB sheathing).

In all of the experiments, only one of the three parallel joists failed because the assemblies were loaded under displacement control (if they had been loaded under force control, the other two joists might have failed following the first one). The first joist to fail was always on one edge of the assembly. Fig. 3.6 shows the location of the first crack that initiated failure in each joist and its approximate pattern.

Based upon the test data, the bending strength, f_b, of the bare joist was calculated to be 3013 psi.

18
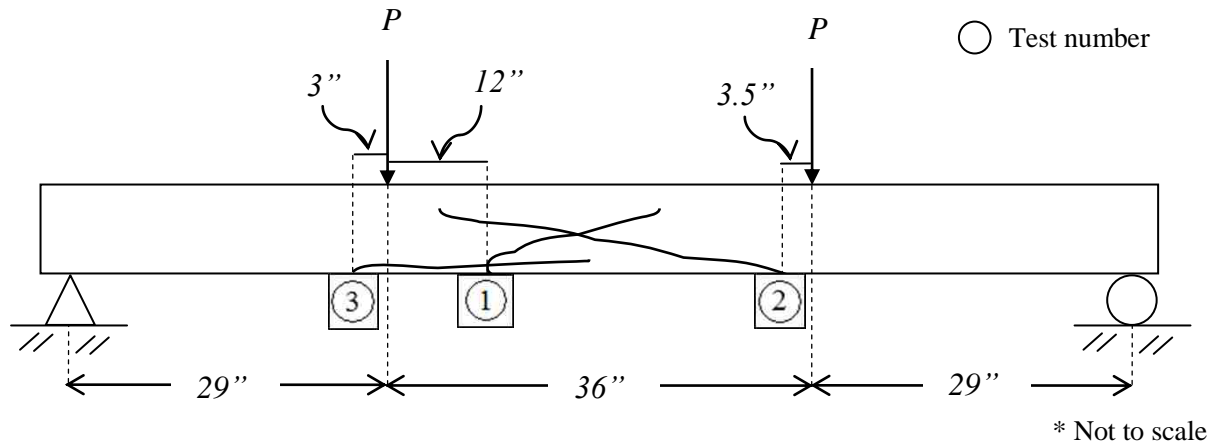
Figure 3.6 Location of initial crack in the wood joists.

In experiments No. 1 and No. 3, the first crack that initiated the bending failure of the joist was located at the location of a knot (shown in Figs. 3.7 (a) and (b)). No knot was detected in the constant moment region in experiment No. 2, but the joist still failed in this region with a bending crack on the tension side of the joist. In assembly No. three the joists appeared to remain bonded to the OSB sheathing at all points, which means the adhesive was strong enough to resist the shear flow acting at the interface between the two members. No apparent yielding in the nails was observed (although there probably was yielding prior to failure).

(a) Test No. 1

(b) Test No. 3

Figure 3.7 Bending failure at the location of a knot.

المنارة للاستشارات

3.2.5   Comparison between tests

The load capacities of the three experiments are shown in Fig. 3.8, where it is also shown that the bare joist was the least stiff, and the glued-and-nailed specimen was both the stiffest and the strongest. Also, it can be seen that the curves are approximately linearly elastic and that there is no evidence of inelastic behavior prior to joist fracture. Thus, it appears that even the nailed connection was behaving in a fully composite manner up to failure. It is actually surprising that the composite specimens failed at much higher loads than the bare section: this would not have been predicted by classical mechanics of materials, which predicts, for all three cases, the same tensile bending stress at the bottom of the joist at midspan where the discontinuity between sheathing panels is located, meaning that the weakest point in the joist is not necessarily located at this section.

In these experiments, a load capacity increase of 73.4% between the bare joists and the joists from the glued-and-nailed assembly, and a 34.5% increase between the bare joists and the joists from the nailed-only assembly, show a higher strength on the tested composite assemblies. Nonetheless, this increase in bending strength could be due to statistical scatter in the bending strengths of the bare joists. Thus, a larger set of experiments was performed to verify this behavior.
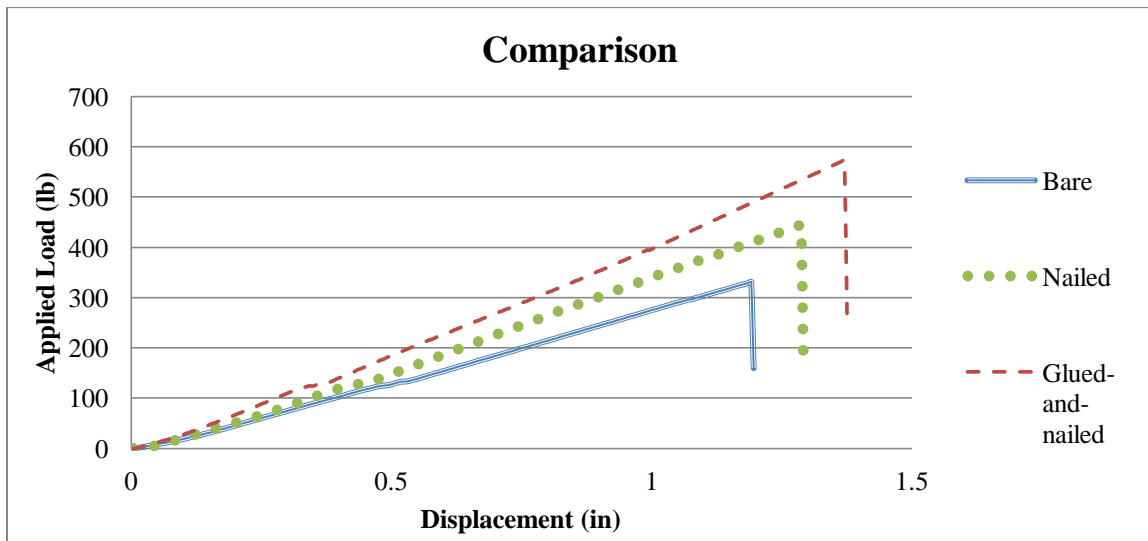
Figure 3.8 Comparison between loading capacities of the three tests.

3.3 Second set of experiments - individual T-beams

Based on the previous results of the assemblies where composite action apparently increased both the stiffness and the bending strength of the joist, a second set of eight flexural tests was performed to provide more data to verify or disprove the hypothesis that composite action increases the bending strength of a wood joist, even with a gap between panels.

3.3.1 Test setup

Taking into account the behavior of the previous experiments, the new specimens were slightly modified. Now it was decided to test only one 2" x 4" x 8' wood joist with two 2'x 4', 7/16" OSB panels on the top to form a T- beam (with a 24"-wide flange and the same 1/8" gap at midspan). In this test setup, the load sharing effects are avoided and only the effects of composite action between the joist and the sheathing are present.

Based on the fact that the weakest point in the previous assemblies was not located at the position of the gap as it was expected, two bare joists and six T-beams (three with a nailed connection and three with nailed-and-glued connection) from a second batch of wood joists were carefully selected with different locations of knots (possible weak points) along their span to test the new hypothesis that the location of the weakest point in the joist with respect to the location of the gap discontinuity plays a key role in increasing the bending strength of the joist due to PCA.

The first three T-beams were only nailed with 8d, 2½" long nails, spaced at 11.5" and with a 1" end distance for the two end nails to two OSB panels (as shown in Fig. 3.9). The next three T-beams were glued-and-nailed using approximately a 1/16'' layer of PL-400 Loctite Semi-structural adhesive at the interface between the joist and the OSB panels. Also, two 2"x 4"x 11.25" wood blocks provided lateral and torsional support to the OSB and to the wood joist at the supports, as shown in Fig. 3.10.

21
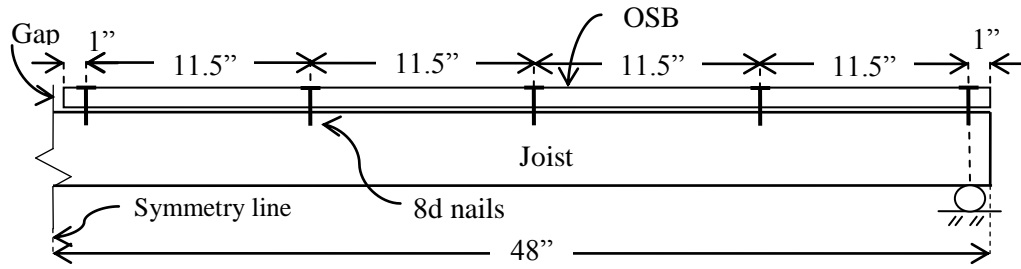
Figure 3.9 Nail schedule for T-beams.

3.3.2 Materials

One 2"x 4"x 8' hem-fir joist visually graded as a stud by the WWPA and two 2'x 4' sheets of 7/16'' thick OSB were utilized per T-beam. Also two 2" x 11" wood joists (to transfer the loads from the actuator), PL 400 Floor and Deck semi-structural elastomeric adhesive for the glued-and-nailed T-beams, 8d-2 ½'' long common wire nails and the MTS Hydraulic Actuator were utilized.

3.3.3 Procedure

Two T-beams with identical characteristics were placed side by side to avoid any instability in the actuator. The T-beams were loaded to failure with the same loading conditions from the previous tests (under four-point bending and under displacement control) as is shown in Fig. 3.10. The same procedure was followed to test the two bare joists.

Figure 3.10 Test setup.

22

3.3.4 Results

As already said, two T-beams were tested side by side, but only one failed due to the material's variability in bending strength (knots with random location and different sizes, slope of the grain, moisture content, etc.) and because loading was under displacement control.

In the same way as in the first experiments of the assemblies, two out of three nailed-only T-beams failed at a location of a knot in the constant moment region as shown in Fig. 3.11, while in the third nailed-only T-beam no knot was detected in this region and failure was initiated at the bottom of the joist three inches away from the gap discontinuity in the sheathing, resulting in a higher strength. This confirms the hypothesis that if no knots are present in the constant moment region, then failure in the joist should occur near the location of the gap discontinuity. The two bare joists and the six T-beams failed under tensile stresses. The load-displacement curve for all specimens again had linear behavior up to failure as shown in Fig. 3.12, which this time shows that an increase in stiffness (as the rigidity of the connection at the interface increases) does not necessarily mean an increase in strength of the tested T-beams.

Figure 3.11 Failure of T-beam at a knot close to the gap in the OSB.

23
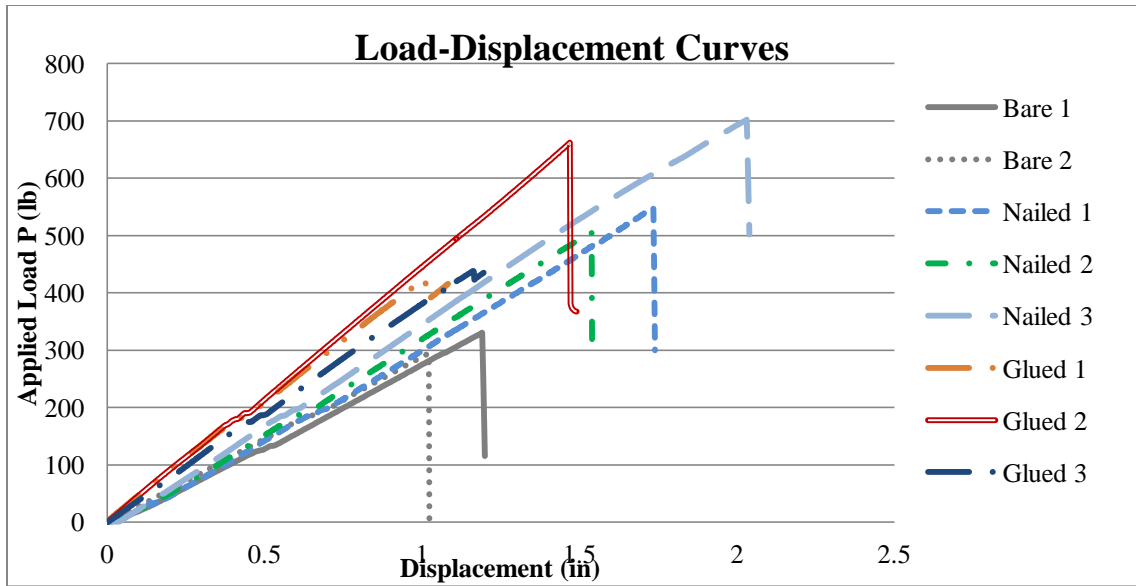
Figure 3.12 Load-displacement curves for tested specimens.

In contrast to the results of the previous set of tests, the strengths of the glued-and-nailed T-beams were not always higher than the nailed-only T-beams, as shown in Fig. 3.13. This is probably due to the different position and size of the knots in the joist. Also plotted in Fig. 3.13, is the allowable load set by the NDS-ASD design code, calculated by using the 675 psi allowable bending stress obtained from the NDS Supplement Table 4A [NDS 2005] (no load factors or excessive deflections were considered). Fig. 3.14 shows a 1.5" knot at less than 2" from the gap location in a glued-and-nailed T-beam, resulting in a much lower strength than a nailed-only T-beam.
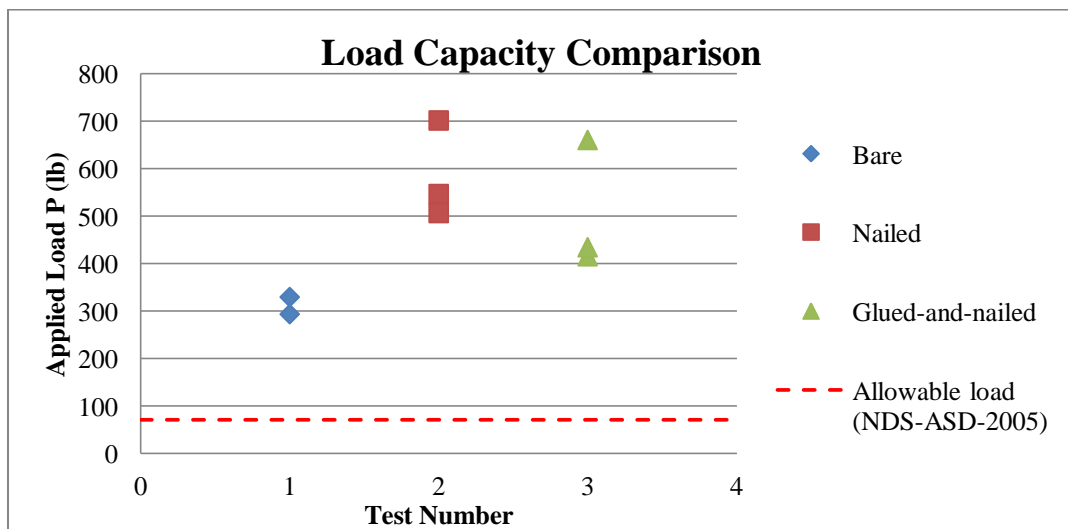
Figure 3.13 Load capacity comparison between tested individual T-beams.

Figure 3.14 Location of the knot at almost the same location as the gap.

Note that a knot below the gap would be the worst-case scenario in achieving any PCA in the T-beam as the gap discontinuity plays a major role in the strength of the joist because the tensile stresses at the bottom of the T-beam increase near the gap discontinuity. Also note that the chance of having the weakest knot close to or at the location of the gap is low, and hence a statistical increase in the strength of the joist might be possible.

3.4 Behavior of nailed and nailed-and-glued connections

The next major concern in determining if there is an increase in the strength of the joist is finding the moment that the OSB panel is capable of resisting at sections away from gap discontinuities and hence, how much the tensile stresses at the bottom of the wood joist are decreased. This contribution can be determined by characterizing the behavior of the connection between the two members. In the experiments described so far, no deformations or yielding in the nails had been observed and the joist appeared to remain bonded to the OSB panels at all sections in all of the flexure tests previously described. However, there could have been small slips that were not noticed. Therefore, direct shear tests, described next, were performed to obtain the load-displacement curves of the nailed connection and the nailed-and-glued connection.

25

3.4.1 Load-displacement properties of nailed joints

3.4.1.1 Test setup

Several researchers have tested joist-to-sheathing connections with different specimen configurations and parameters. Mohammad [Mohammad 1994] proposed a test method to obtain the interlayer slip behavior of the nails under cyclic loading and moisture content changes in OSB-to-lumber connections. This method was later utilized by Wang [Wang 2009] and Mi [Mi 2004]. Mi tested ten specimens of spruce pine fir (SPF), connected to 7/16" OSB panels with 8d nails under tension load applied parallel to the grain of the lumber, as shown in Fig. 3.15, developing a multi-linear model for the load-displacement curve based in his results. Mi's specimen was utilized in this research at constant moisture content conditions, varying only the species of the lumber (douglas-fir with almost the same specific gravity as SPF) and loading the specimen under compression forces to compare the load-displacement curves.
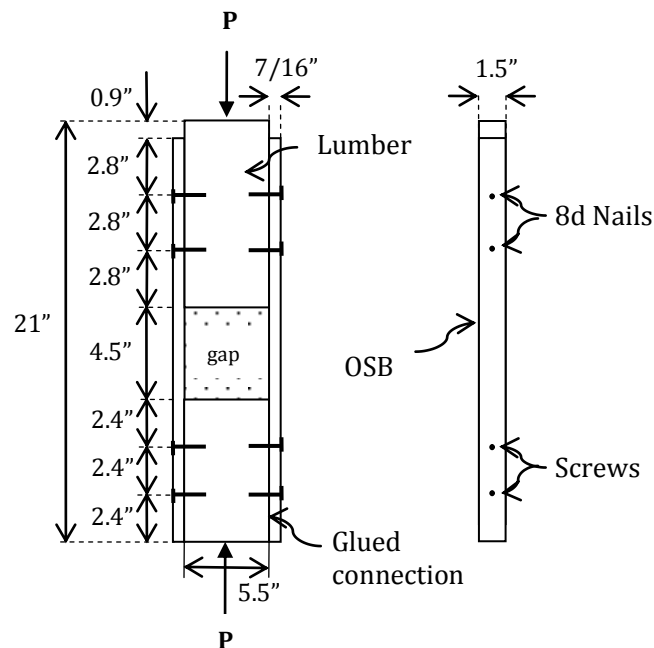
Figure 3.15 Direct shear test setup.

The specimen had two different ends, one "test" end with the nails to be tested and one "dummy" end, with screws and a glued interface to prevent slip. The dimensions

www.manaraa.com

of the components are shown in Fig. 3.15. The strands of the OSB were oriented perpendicular to the direction of the load (as in a typical roof assembly under bending moments with the strong axis of the OSB perpendicular to the longitudinal axes of the joists). All members were selected to be free of defects in the area where the nails were driven.

3.4.1.2 Procedure

Two specimens were loaded by the Bionix testing machine, applying a displacement controlled loading with a rate of 0.0197 in/min (0.5 mm/min), and recording load and displacement measurements every second, using a data acquisition system. Also a dial gage was installed in the specimens as shown in Fig. 3.16 to measure the slip between the OSB and the lumber at a location closer to the nails at the test end. Readings of this interlayer slip were recorded every 30 seconds and compared with the overall deformation recorded by the machine.

Figure 3.16 Specimen for testing connection behavior.

27

3.4.1.3 Results

The resulting load-displacement curves for both specimens are shown in Fig. 3.17. The force plotted in this figure was obtained by dividing by four the total force applied to the specimen. The difference in slip between the curve obtained from the data acquisition system and the curve obtained from the dial gage is attributed to seating effects when transferring the load from applied by the testing machine to the wood blocks.
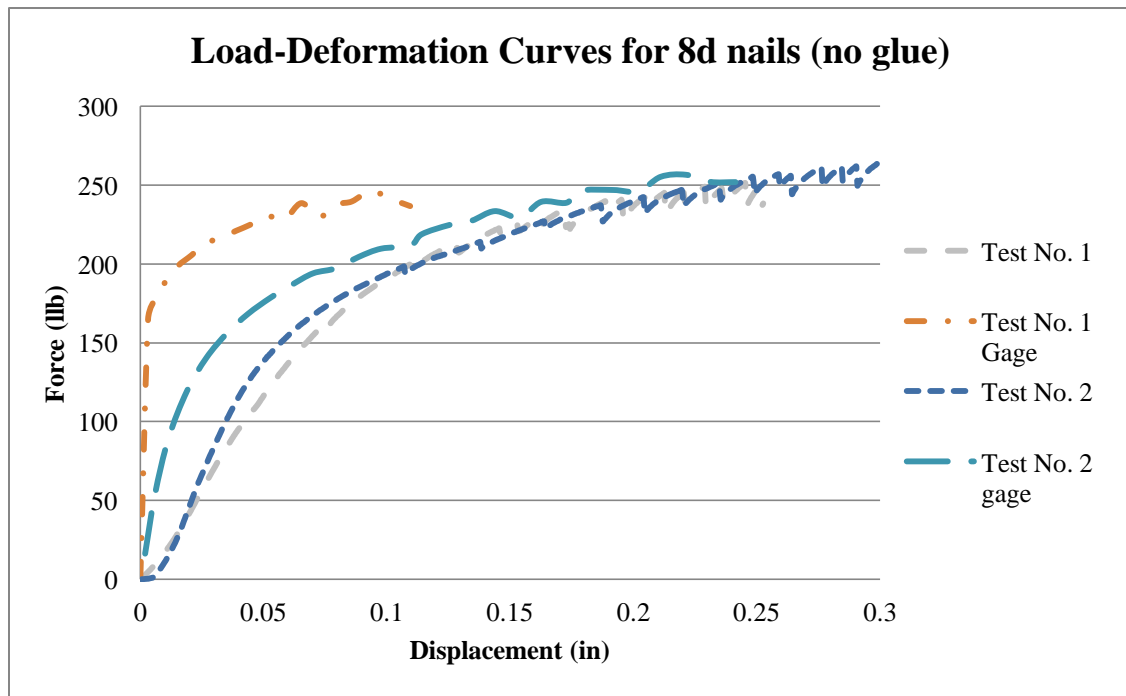
Figure 3.17 Load-deformation curves for 8d nails and douglas-fir lumber.

A comparison between the resulting load-deformation curves from test No. 2 and the multi-linear model for the load-displacement curve developed by Mi [Mi 2004], for one nail, are shown in Fig. 3.18.
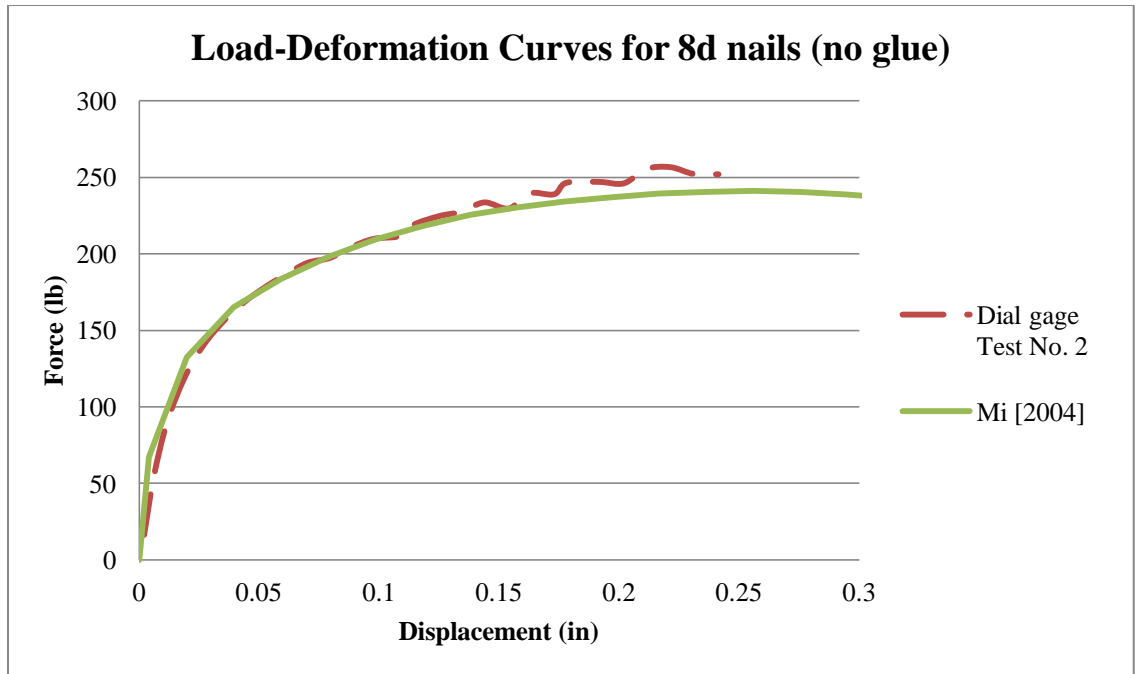
Figure 3.18 Comparison between Mi's curve and Test No. 2 curve.

As it is shown in Fig. 3.17, the curve obtained from the dial gage from test number two follows very closely the curve from Mi, as the slips were recorded at the location of the nails.

3.4.2   Load-displacement properties of glued-and-nailed joints.
3.4.2.1 Test Setup

A third specimen built to test the glued-and-nailed joint is shown in Fig. 3.19. The same dimensions shown in Fig. 3.15 were used, with the only difference being a 2" gap between the wood blocks instead of a 4.5" gap as in the previous test to avoid a premature failure of the OSB due to buckling. The same nail schedule as in the previous test was used, along with elastomeric semi-structural adhesive at the interface between the members, which was applied with the same procedure as in the flexure experiments.

29

3.4.2.2 Procedure

Axial displacement was controlled by the Bionix testing machine and was applied to the sample with a displacement control, using a rate of 0.019 in/min (0.5 mm/min).
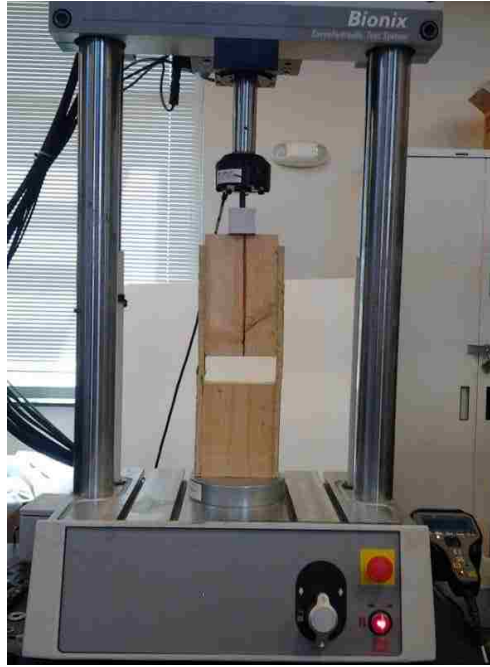
Figure 3.19 Test specimen for glued-and-nailed connection.

3.4.2.3 Results

In this experiment, the displacements were directly obtained from the data acquisition system only. The OSB failed first in what appeared to be buckling effects at the location of the gap between the two wood blocks due to the applied compressive force before the glued interface could fail, as shown in Fig. 3.20, meaning that the glued-and-nailed connection was strong enough to resist the shearing forces at the interface and the OSB buckled first.

30

Figure 3.20 Failure of specimen with a glued-and-nailed connection.

A comparison between the load-displacement curves for the nailed joint (obtained from the dial gage) and the glued-and-nailed joint (obtained from the data acquisition system) is shown in Fig. 3.21. The seating effects were subtracted out of the curve for the glued-and-nailed connection. The forces from the curves for the nailed connection were multiplied by four to compare it to the glued-and-nailed connection. As shown in this figure, the displacement at failure of the glued-and-nailed specimen was high enough for the nails to have a non-linear behavior. The effective linear stiffness of the glued-and-nailed connection was determined to be 31,286 lb/in.
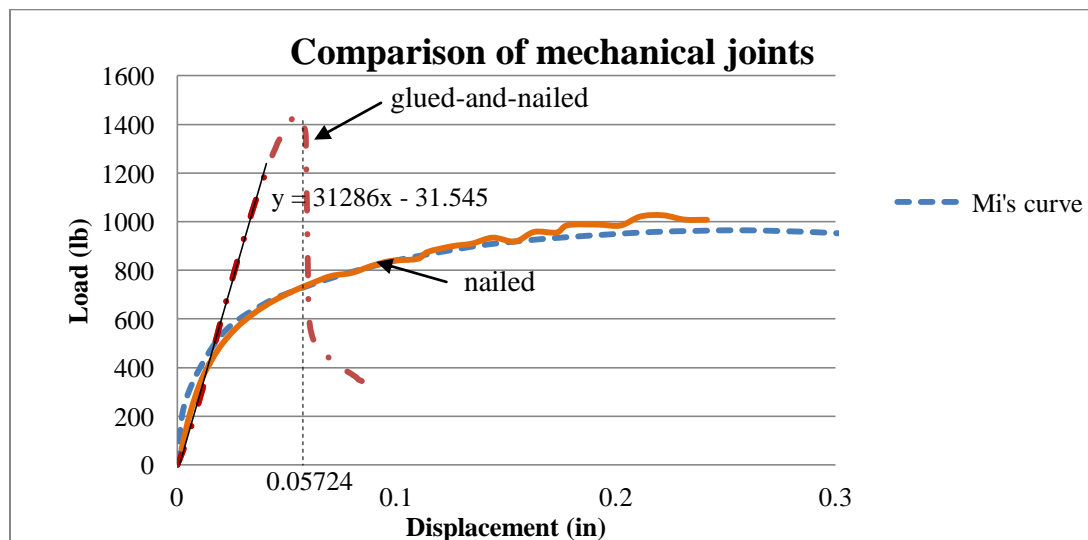
Figure 3.21 Comparison between nailed and glued-and-nailed connections.

31

3.5 Third set of experiments - individual T-beams with similar properties

A third and final set of tests of individual T-beams was performed. Now three nominal 4"x 4" wood joists were selected carefully, trying to have knots in different locations along the span that would go as straight and as perpendicular as possible across the transverse section of the joist. The purpose of this selection is to cut the 4"x 4" nominal (3.5" x 3.5" actual dimensions) joists into two 2"x 4" nominal (1.5" x 3.5") wood joists as shown in Fig. 3.22 to produce the minimum difference in strength between the two joists, allowing both joists to have nearly identical bending properties.

Figure 3.22 Two 2"x 4" joists cut from a 4"x 4" joist.

3.5.1   Test setup

A four-point bending test was again utilized, but this time with a larger constant-moment region as shown in Fig. 3.23.
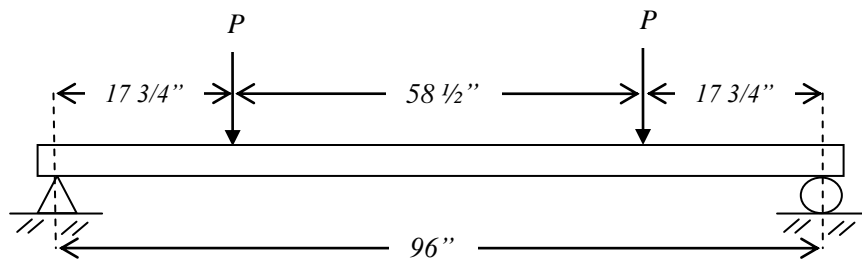
Figure 3.23 Four-point bending test.

32

Each of the two 2"x 4" joists obtained from the 4"x 4" joist were tested separately. The first 2"x 4" joist was tested as a bare joist to obtain the "bare joist strength", while the second 2"x4" joist was tested as part of a T-beam, using again two 7/16" x 2'x 4' OSB panels, and having a gap at midspan to obtain the "T-beam strength", as shown in Fig. 3.24.
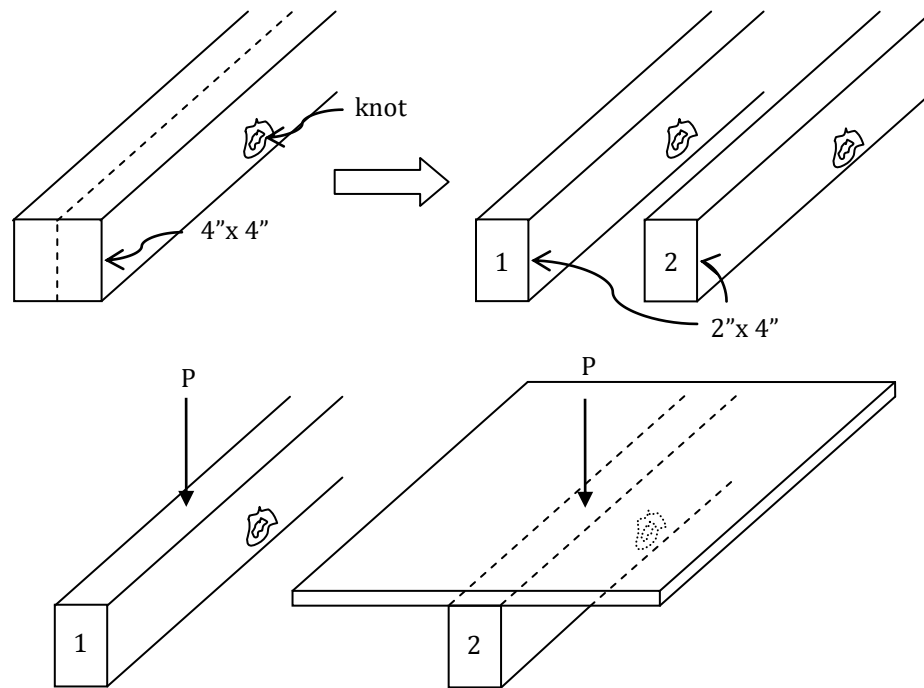
Figure 3.24 Schematic of the procedure.

This procedure was designed to isolate the effects of the PCA when comparing the behavior of the specimens. The nail schedule is shown in Fig. 3.25. It was decided to add glue to the interface only from the point loads to the supports of the joist (where shear forces generated from the external loading exist) to provide a rigid connection in this region, developing FCA, and to prevent any differential displacement (slip) between the joist and the OSB panel towards each end of the joist, forcing the slip to occur only at the nails close to the location of the gap at midspan.

33
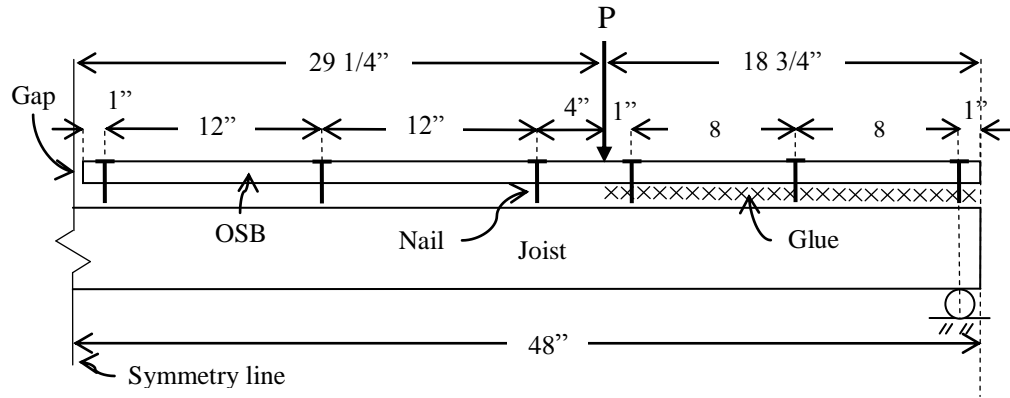
Figure 3.25 Connection at interface of T-beam.

An initial gap of 0.20" was provided between the OSB panels. A dial gage was attached to the top of the OSB (shown in Fig. 3.26) to measure the gap closure at midspan when the T-beams were loaded.

Figure 3.26 Dial gage installed at the gap discontinuity.

3.5.2 Materials

One 4"x 4"x 8' Douglas-Fir joist visually graded as No. 1 joists by the WWPA and two 2'x 4' sheets of 7/16'' thick OSB were utilized per pair (bare joist and T-beam). Also two 2" x 6" wood joists (to transfer the loads from the actuator), PL 400 Floor and Deck semi-structural elastomeric adhesive, 8d-2 ½'' long common wire nails, four 2'' x

4'' x 11.25'' pieces of wood per T-beam (to provide lateral bracing to the OSB at supports), and the MTS hydraulic actuator were utilized.

3.5.3 Procedure

A bare 4"x 4" joist was utilized stabilize the actuator and to force the bare 2"x 4" joist or the T-beam to fail first during the test, as shown in Fig. 3.27.

An axial displacement rate of 0.10 in/min was applied by the actuator.

Figure 3.27 Test setup.

The bare joist was tested first to obtain its load-displacement relation. Then the T-beam was loaded to the same failure load as the bare joist. Prior to failure, the gap was measured with a Vernier caliper. Also, readings from the dial gage were obtained every 30 seconds. Then the T-beam was loaded to failure.

3.5.4 Results

The failure load P for all of the tested specimens is shown in Fig. 3.28.
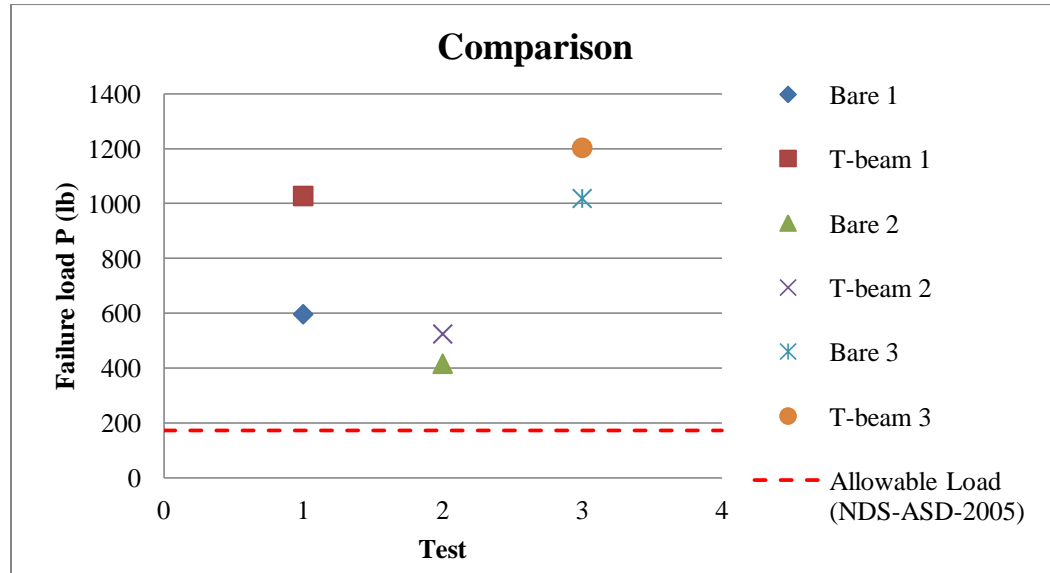
Comparison

Figure 3.28 Failure load comparison between specimens.

As shown in Fig. 3.28, for each pair of 2"x 4" joists, the T-beam was stronger than the bare joist. The load-displacement curves for the pair of 2"x 4" joists from test No. 1 are shown in Fig. 3.29, where the difference in stiffness and in failure loads between the bare joist and the T-beams is shown. An increase in stiffness is evident in the curve of the T-beam before failing. This is confirmed by the readings from the dial gage at the location of the gap, which showed that the gap had completely closed when the T-beam reached its bending strength. This means that some continuity of the top flange was present and the OSB began carrying higher compressive forces, and hence, a larger percentage of the total external moment. It is important to note that in the previous set of individual T-beams described in Section 3.2 (with joists with a lower bending strength) the joist failed before the gap could close in all of the specimens, meaning that the higher the bending strength of the bare joist, the more likely the 1/8" gap is going to close completely, as the T-beam will have a greater curvature and a greater slip in the nails. The failure of both the bare joist and the T-beam occurred at the same knot, which was located in the constant moment region.

36
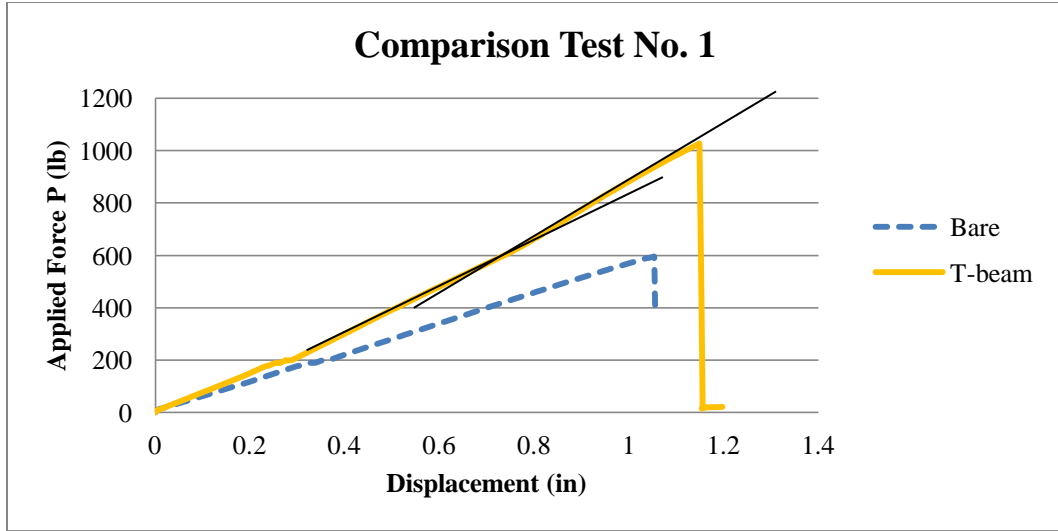
Figure 3.29 Load-displacement curves for test No. 1.

Taking into consideration that the grade of the joists in these three tests is higher, it was decided to increase the width of the gap to avoid a complete closure again. In test No. 2 the initial gap width was increased to 0.40". As shown in Fig. 3.30, both the bare joist and the T-beam failed at lower strengths than in test No. 1, with a total slip of 0.050 inches on each side of the gap (the 1/8" gap would not have closed at this slip). The bare joist failed in bending at the location of the biggest knot, which was located outside the constant moment region, while the T-beam failed at a smaller knot within the constant moment region.
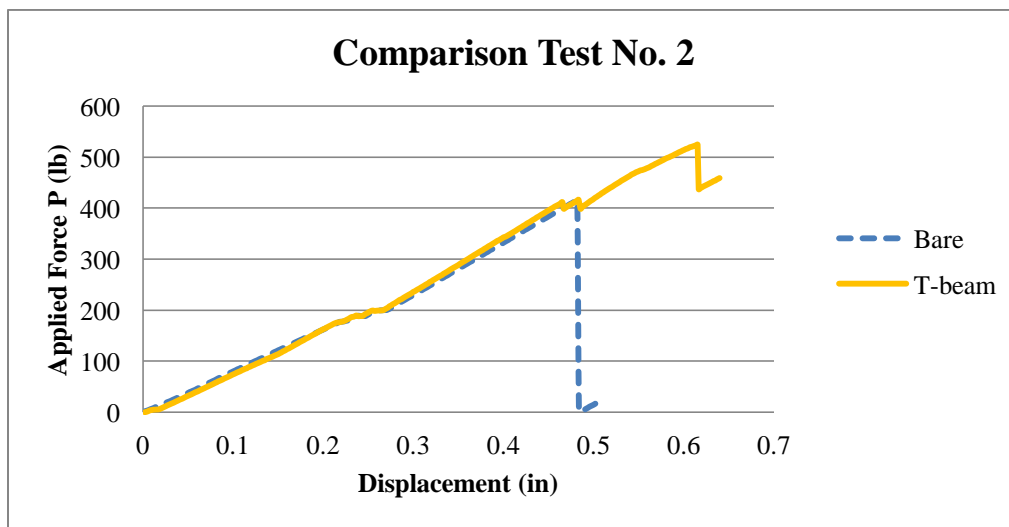
Figure 3.30 Load-displacement curves for test No. 2.

37

The same procedure was followed for test No. 3, providing an initial gap of 0.40"
between OSB panels. As shown in Fig. 3.31, both strengths for the bare joist and the T-
beam are the highest of the three tests, resulting in a slip of 0.129" on each side of the gap
(the 1/8" gap would have closed). No knots were detected throughout the whole constant
moment region, resulting in higher strengths for both tested specimens. Note how the
stiffness of the bare joist and the nailed T-beam remains almost the same, and no increase
in stiffness is observable as shown in Figs. 3.30 and 3.31.
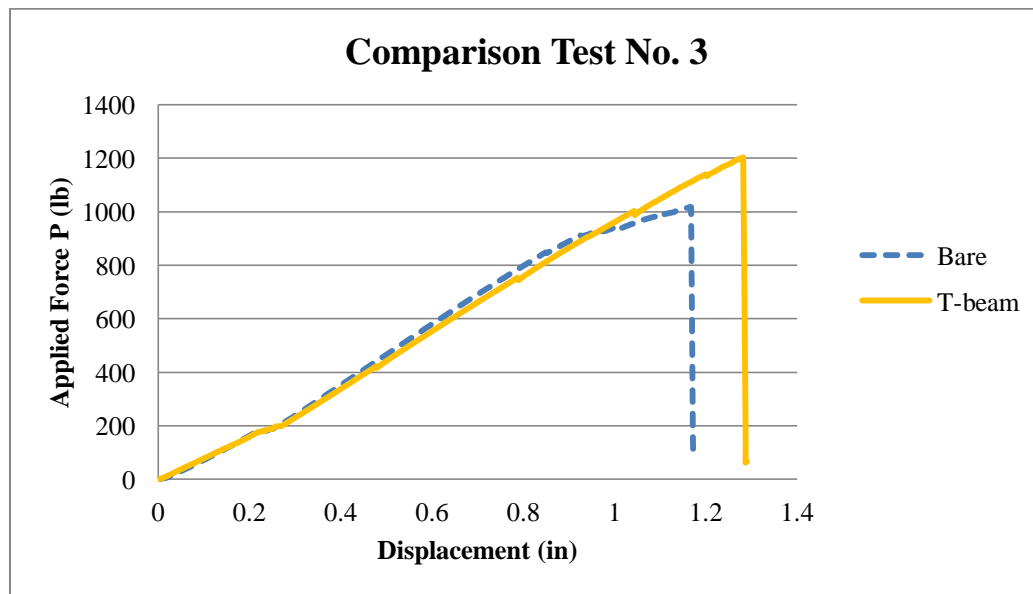
Figure 3.31 Load-Displacement curve for test No. 3.

3.6 Conclusions

According to the results of all of the flexure tests, there appears to be an increase in
the strength of the joist when OSB panels are attached to its top face even when using a
non-rigid connection like a nailed joint. A possible explanation for this strength increase
is that wood has a highly variable bending strength along the length of the joist, mainly
depending upon the locations and the size of knots (some other effects like slope of grain,
moisture content, etc also have an effect), which are weak points. Thus, if the weakest
knot which initiates failure is not located near the location of the gap between panels, this
knot will experience a lowered stress due to PCA. Of course, knot size and location with

respect to gap location between panels is random, and thus statistics must be brought to bear on the problem.

Other important factors that might be affecting this strength increase and that need to be taken into consideration in further analyses are: gap width between OSB panels, the structural grading of the bare joist (as it limits the size and location of the knots for higher grades), and the load-displacement behavior of the joint, which will determine the magnitude of the axial force being carried by the flange. Analytical and numerical analyses investigating the mechanical behavior of the T-beam with PCA considering all of the factors described above are described in Chapter 4, while statistical effects are investigated in Chapter 5.

Chapter 4   Analytical and Numerical Analyses

4.1 Introduction

The following analytical and numerical analyses were conducted based on the fact that an increase in the bending strength of wood joists nailed to OSB sheathing when a gap is present in the flange of the T-beam was not considered in previous research (as mentioned in Chapter 2) but as shown in the results of the laboratory experiments, an increase in the bending strength of the T-beam was still observed.

4.2 Theoretical development

A general approach is considered first.

With reference to Figs. 4.1 and 4.2, consider a 2"x 4"x 8' wood joist attached to two 7/16"x 2'x 4' OSB panels with a gap discontinuity at midspan (same as the T-beams from the experiments), with an even 11.5" spacing of the nails along the joist (to produce a symmetrical distribution of the nails), with an edge distance of 1" at the ends of each OSB panel (no glue). Also consider that the T-beam is subjected to an external constant moment at each end, and that the width of the flange of the T-beam, b_f, is equal to 24", which is the typical distance between joists in roof assemblies.
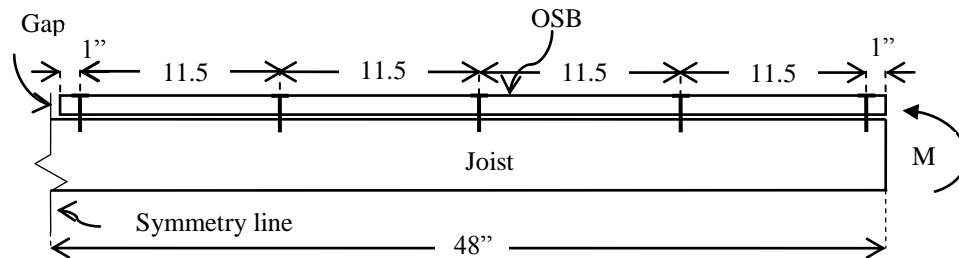
Figure 4.1 Wood joist/sheathing parameters.
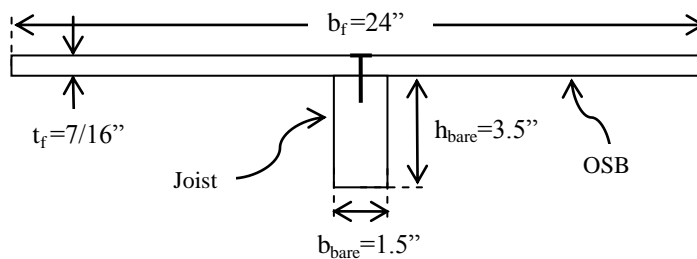
Figure 4.2 Section of composite T-beam.

40

Although the joist is only under constant moment, some shear flow is generated at the interface between the two members because of the changing axial force being carried by the flange of the T-beam, which is equal to zero at each free end of the panel, due to the gap discontinuity (as shown in Fig. 4.3). The magnitude of the compression force generated in the flange, F_f, is a function of the load-displacement properties of the nails.
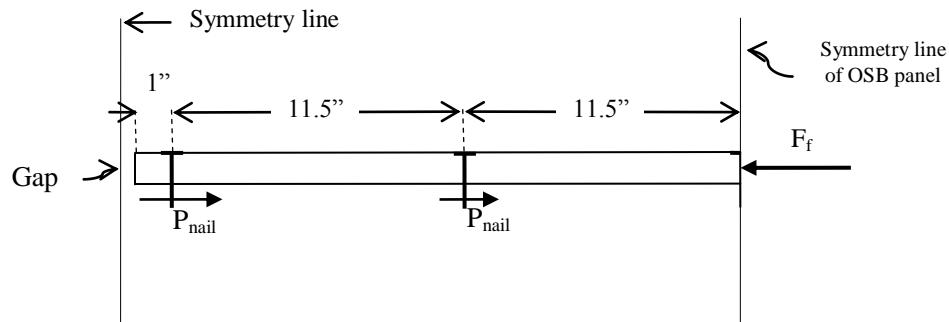
Figure 4.3 Free-body diagram of the OSB panel.

When the T-beam section is bent, and because of the non-rigidity of the nailed connection, a differential slip will occur between the web and the flange, with the two end nails in each OSB panel having the largest slip, meaning that these two nails are the first to start yielding (behavior also reported in previous research by Wolfe [1990, 1991]). Meanwhile, the interior nails either carry smaller forces than the end nails (in the elastic or plastic limits of the nail load-displacement curve) because of a smaller slip, or do not carry any force, as with the center nail in the OSB panel, due to symmetry.

Two limiting cases can be considered. The first case is described in Section 4.3 and it is present when the flange and the web are assumed to be fully composite, as shown in Fig. 4.4(a). In this case the nails are assumed to be only linear elastic and to resist the generated shear forces at the interface. The second limiting case is described in Section 4.4 and it is present when the forces of the nails being transferred to the flange are small, so that the flange can be considered as axially infinitely stiff (as will be explained later), and the slip at the end nails can be estimated as the axial deformation of the bare joist, as shown in Fig. 4.4(b).

41
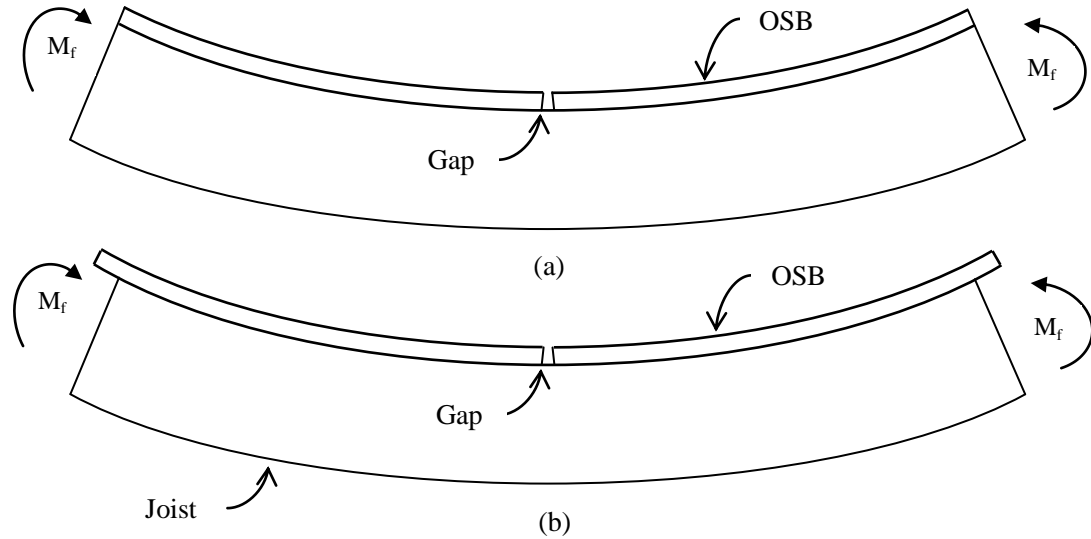
Figure 4.4 Upper and lower bound conditions for connection behavior.

4.3 First limiting case – full composite

Because of the complexity of the behavior of the T-beam when considering the effects caused by the gap in the flange and the non-rigid interface connection (slip of the flange due to the constant stiffness of the nails is present in this case), a finite element analysis (FEA) was performed.

The commercial software SAP2000 was utilized to create the finite element model. A mesh of 0.25"x 0.2188" four-noded thin shell elements was used to model the wood joist and the OSB sheathing with the same dimensions and parameters shown in Figs. 4.1 and 4.2. The properties of the flange were obtained from design tables M9.2.1 and M9.2.4 for OSB [NDS, 2005] assuming it is stressed in the strong direction, while the properties for the wood joist were obtained from Table 4A from the NDS supplement [NDS 2005]. Mirror symmetry was employed to model the gap discontinuity in the flange of the T-beam, as shown in Figs. 4.5 and 4.6:

42
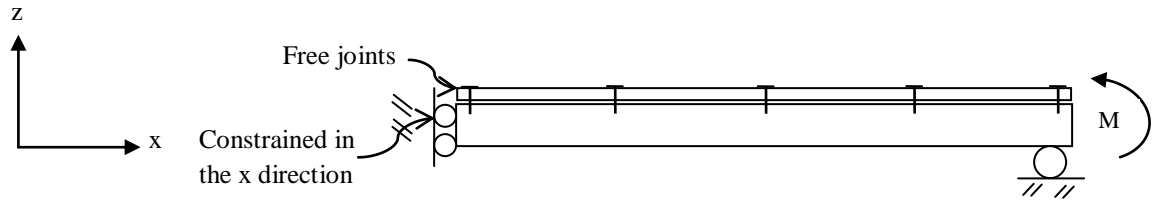
Figure 4.5 Boundary conditions for FEA.
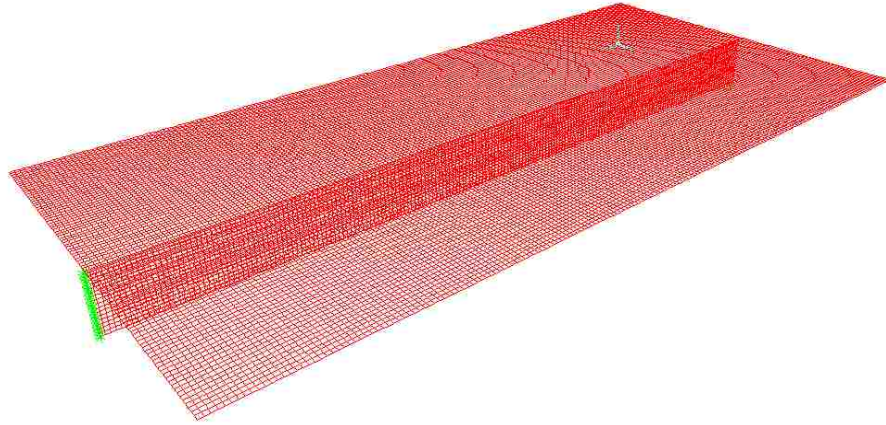
Figure 4.6 3-D view of the T-beam.

A 7/32" gap was left in the longitudinal axis of the T-beam between the web and the flange so that they behave independently, without any common joints, as shown in Fig. 4.7. The nails were the only connection between the OSB panels and the joist. They were modeled as frame elements with linear stiffness, a diameter of 0.131" (8d nails), a length of 2", connected to each joint, spaced at every 11.5", and with 1" end distance measured from the ends of the panels, as shown in Fig. 4.8. Finally, Fig. 4.9 shows an extruded view of the T-beam cross-section, showing the shell and frame elements and their respective thicknesses.
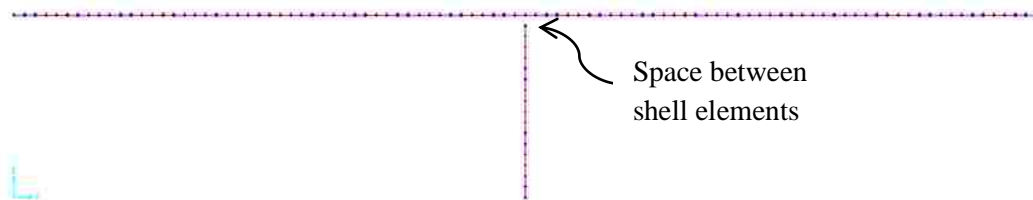
Figure 4.7 Cross-sectional view of FEA model.

43
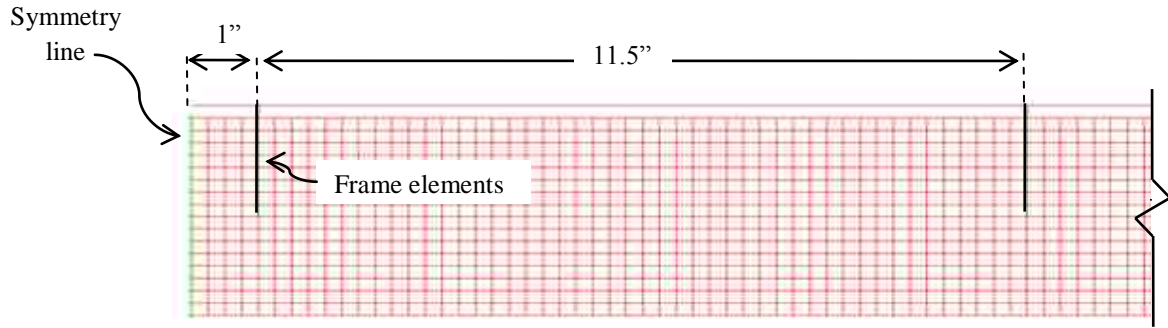
Figure 4.8 Side elevation view showing frame elements connecting flange and web.
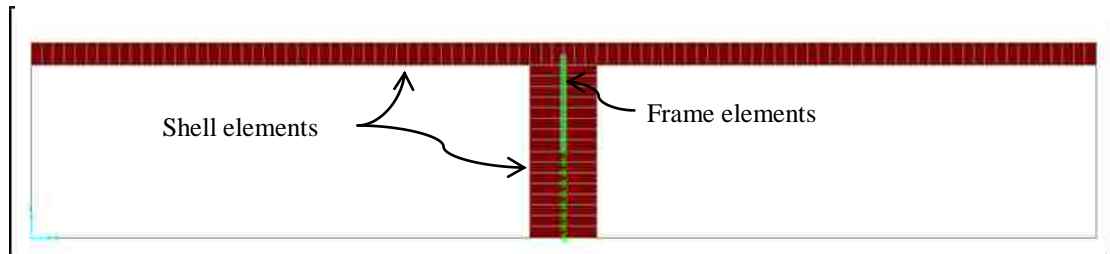
Figure 4.9 Extruded view of the T-beam cross-section.

An external moment, M_f, was applied at a joint located at the right end, at mid-height of the joist in the finite element model as a concentrated moment. This moment at failure was calculated from a typical bending strength of the wood joists obtained from the laboratory experiments described in Section 3.2 and is given by

$$M_f = F_b S_{bare} = (3000 \text{ lb/in}^2)(3.0625 \text{ in}^3) = 9187.5 \text{ lb-in. } M_f = F_b S_{bare}$$

The shear force carried by each nail close to the gap location resulting from the FEA is shown in Fig. 4.10. As mentioned before, if the nails are assumed to remain linearly elastic, this shear force is approximately 1.61 kips (this force is much higher than the nail yield strength as shown in the load-displacement curve from Fig. 3.18). Also from this analysis, the second nail carries a shear force of 0.678 kips, which is still greater than the yield strength of the nails, while the third nail (center nail in the OSB panel) does not carry any shear force due to the equilibrium of forces in the flange.

44
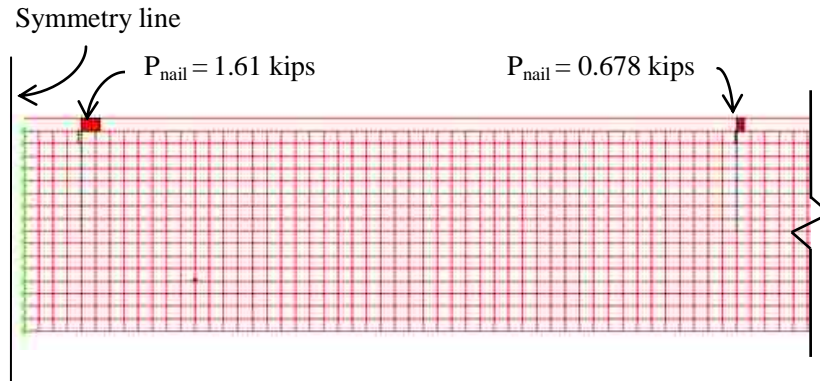
Figure 4.10 Shear force at edge nail close to gap location, from FEA.

This analysis shows that the nails would have yielded by the time the T-beam reached its failure load and also shows that a full composite action cannot be achieved because the nail behavior will be nonlinear and NPCA will be developed. Also the FEA shows that the flange will not be under uniform stresses along its cross section, creating a shear lag effect, as shown in Fig. 4.11.
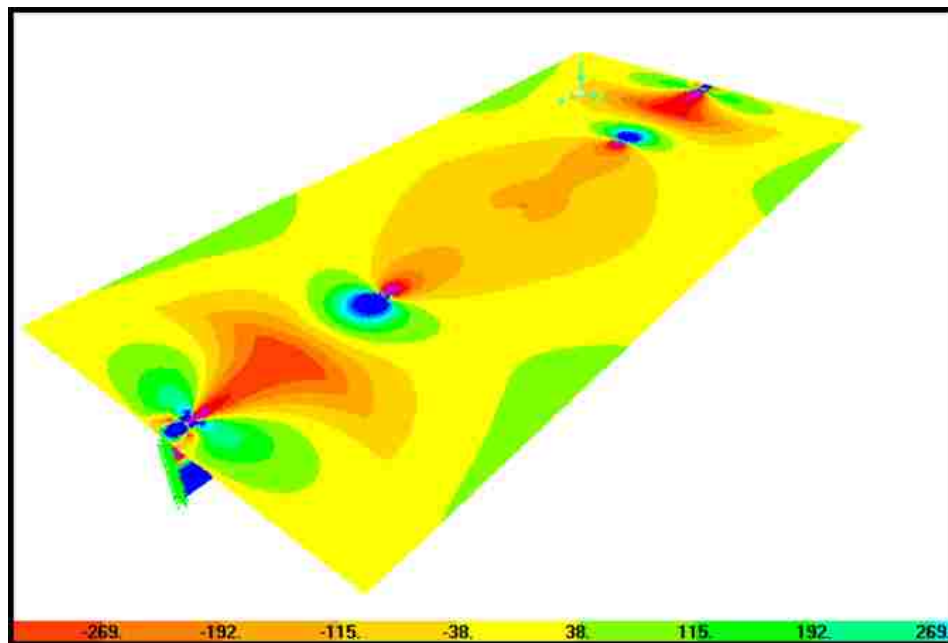
Figure 4.11 Contour plot of the axial bending stresses, σ_{xx} (psi), showing the shear-lag effect in the flange of the T-beam.

Finally, Fig. 4.12 shows that the tensile stresses at the bottom of the joist at the location of the gap (at the symmetry line) are still lower than the expected bare joist stresses (3000 psi). Although in this analysis the nails are considered to be linear elastic, this lowered tensile bending stress in the joist is also present when the nails are considered to be yielding, as it will be explained in Section 4.5.

Location of nail

Bottom tensile stress < 3000 psi (bare joist analysis)
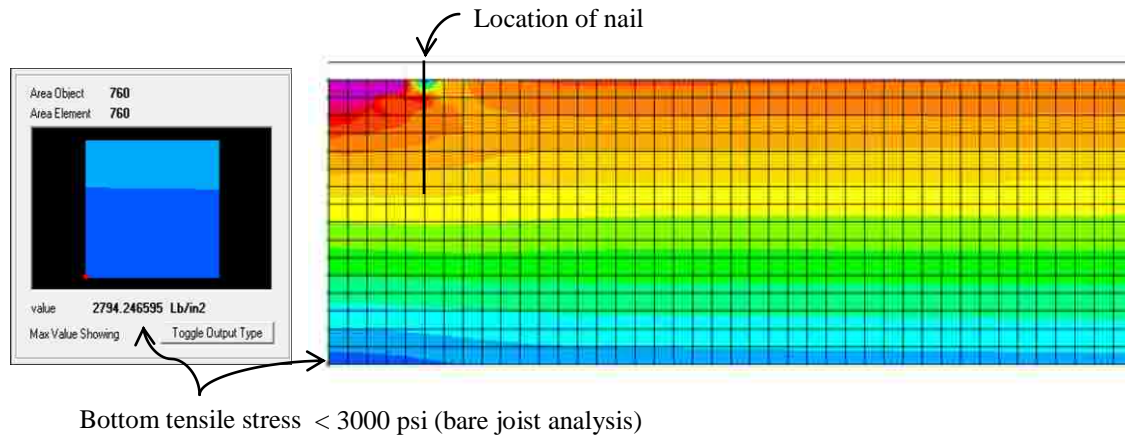
Figure 4.12 Reduction in tensile stresses at the location of the gap.

4.4 Second limiting case – rigid flange

Another approach that can also be utilized to confirm that the end nails in the OSB panel will yield when failure loads are applied to the T-beam, is to estimate the shear forces in the nails with reference to the load-displacement curve by calculating the differential slip at the nails. Some approximate methods have been developed to calculate this interlayer slip; one of them was developed by McCutcheon [McCutcheon 1986], who utilized a fairly simple approach to approximate linear slip. A high level of accuracy in the calculation of the interlayer slip is only needed when the nails are carrying forces in the non plastic region. However, when failure loads are applied to the T-beam, the interlayer slip the nails may be in the plastic region of the load-displacement curve and the high accuracy of the interlayer slip is no longer needed, as the forces being transferred by the nails will remain almost constant. A simplified analysis is presented here to get an approximation of the interlayer slip of the nails and show that their behavior will be plastic.

46

In the following, the joist and the sheathing are assumed to be axially infinitely stiff, and assume the T-beam is under constant moment, M_f.
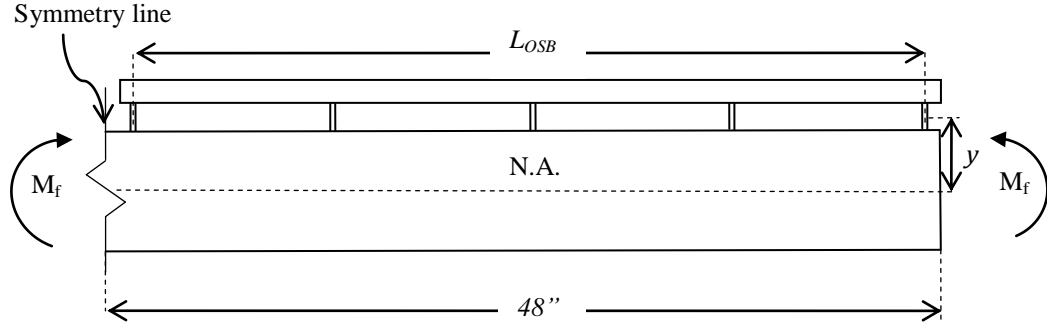
Figure 4.13 Joist/sheathing model to estimate forces at nails.

The normal strain and radius of curvature in the joist are

$$\varepsilon_{xx} = \frac{-y}{\rho}, \text{ and} \tag{4.1}$$

$$\rho = \frac{E_j I_b}{M_f}. \tag{4.2}$$

$\Delta_{nail_{end}}$ is the nail slip at the ends of the OSB panel,

$$\Delta_{nail_{end}} = \varepsilon_{xx} \frac{L_{OSB}}{2}, \tag{4.3}$$

substituting Eqs. (4.1) and (4.2) in Eq. (4.3)

$$\Delta_{nail_{end}} = \frac{M_f y L_{OSB}}{2 E_j I_b}, \tag{4.4}$$

where

L_{OSB} is the distance between end nails of the OSB panel,

y is the distance from the neutral axis of the bare joist to the interface of the T-beam,

E_j is the modulus of elasticity of the bare joist, and I_b is the moment of inertia of the bare joist.

47
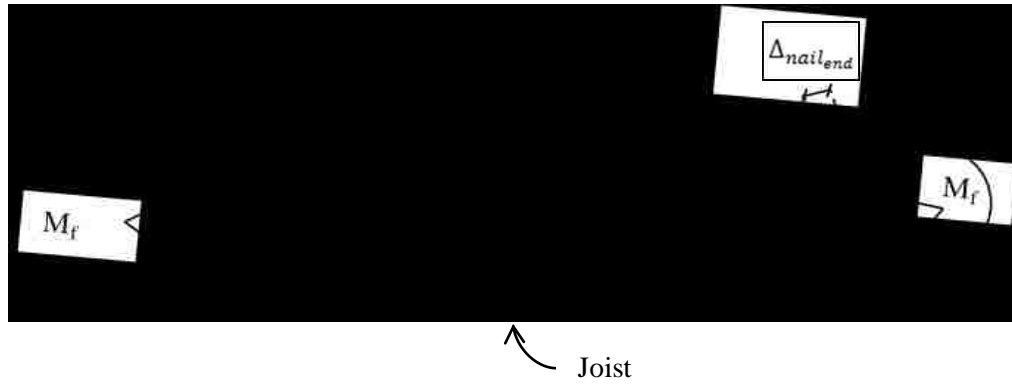
Figure 4.14 Deformed shape of T-beam.

Considering the strengths of the bare joists in the third set of experiments from Section 3.5, the predicted slips of the end nails were calculated and plotted with reference to the load-displacement curve of 8d nails in Fig. 4.15 as follows:

$$\Delta_{nail} = \frac{(M_f)(1.75\ in)(46\ in)}{2\left(1200\ {kips}/{in^2}\right)(5.3593\ in^4)}\ .$$
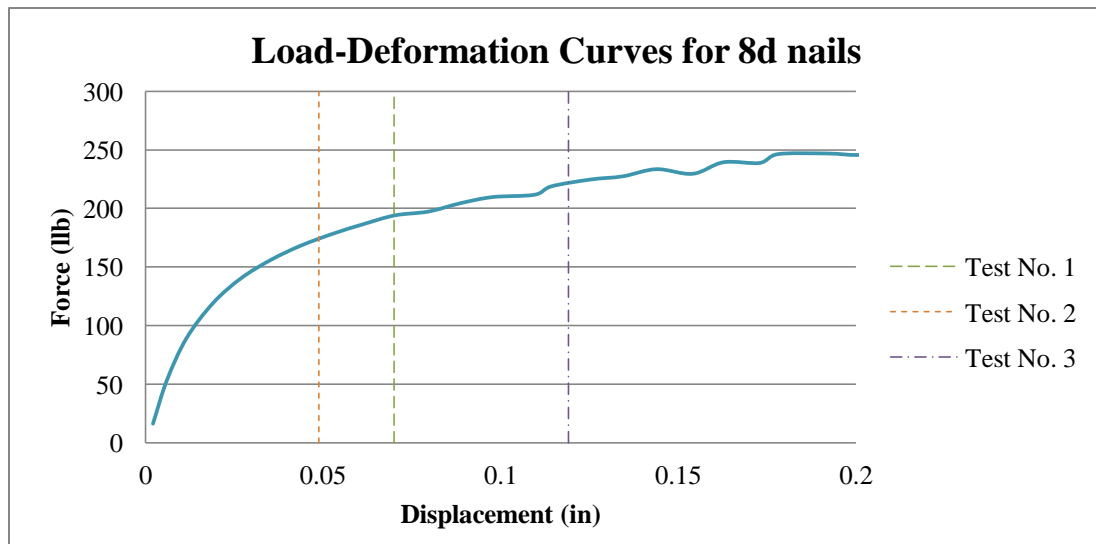
Figure 4.15 Force being carried by the nail.

As shown in Fig. 4.15, even for the weakest joist (with Fb = 2540 psi and a predicted slip of 0.0486) the displacement is in the nonlinear region of the curve, transferring an approximate force, P_{nail}, of 175 lb to the flange. This force will slightly increase as the strength of the joist increases (meaning that greater slips will be obtained

according to Eq. (4.4) and as shown in Fig. 4.16) due to strain hardening in the load-displacement curve of the nails.
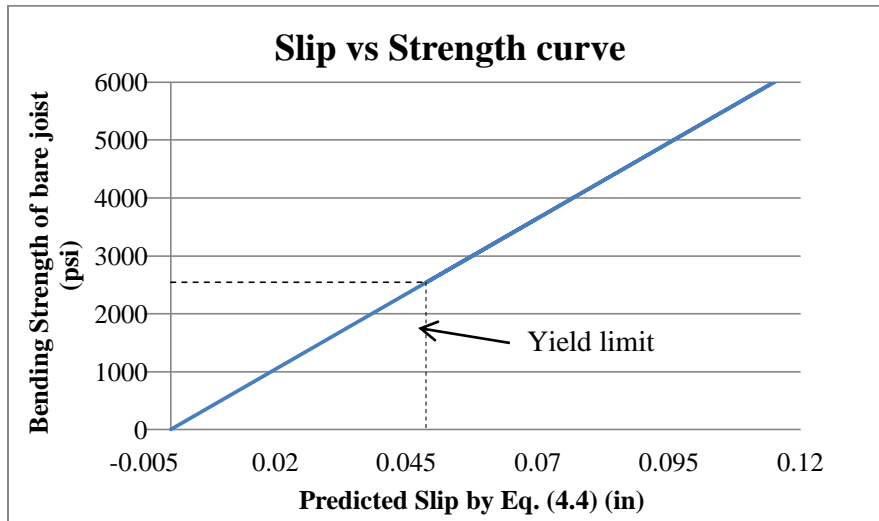
Figure 4.16 Strength-predicted slip relationship.

Thus the force being transferred to the flange varies nonlinearly with slip. Load-displacement relations for different joint patterns have been modeled to get the value of the force at a specific slip accounting for the nonlinear behavior of the nails [McLain 1976, Pellicane et al. 1991, Wang 2009, among others]. However, if this 175 lb force is taken into consideration as a conservative lower bound value for the yield strength of the nails of a elastic-perfectly plastic model for the analysis of NPCA, then it can be assumed that a constant concentrated force will be transferred by the nail to the flange. Nonetheless, this 175 lb force is much higher than the current allowable nail shear forces set by the NDS based on the yield model theory [Aune, Patton-Mallory, 1986] (around 85 lb for 8d nails) and the 0.05" displacement limit is also greater than the 0.015" limit utilized for several years as the approximate proportional limit to calculate the allowable nail force by the NDS prior to 1991.

This force of 175lb being transferred by each end nail to the flange would be consistent with the assumption of the flange being axially infinitely stiff, as the force being transferred is low and the axial deformation of the flange can be neglected, which

49

according to the load-displacement curve of the nails, this second limiting case is closer to the actual behavior of the T-beam than the first limiting case.

4.5 Nonlinear partial composite action (NPCA)

For 2"x 4" wood joists with bending strength higher than 2500 psi, the slips will be high enough to yield the nails and an idealized concentrated constant force of 175 lb may be assumed to be acting on the bare joist at the location of each end nail. Because of the uncertainty of how much force the interior nails are able to develop (they may/may not yield), these interior nails can be conservatively neglected.

Neglecting the interior nails for simplicity, a second analysis is performed with the same parameters as before, but in this case, only two end nails on each 48" OSB panel are assumed, as shown in Figs. 4.17 and 4.18.
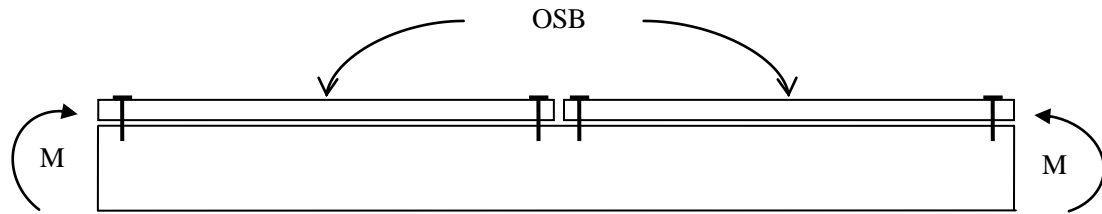
Figure 4.17 Joist with only one gap in the sheathing.
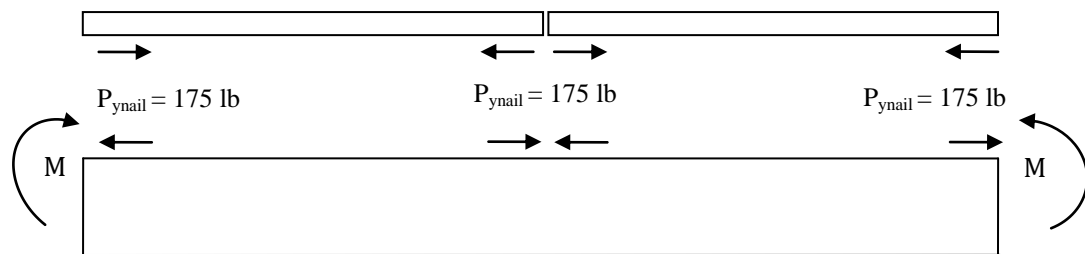
Figure 4.18 Free-body diagram of the joist and OSB sheathing after nails have yielded.

Using superposition, the free-body diagram of the wood joist shown in Fig. 4.18 can be separated in two cases:
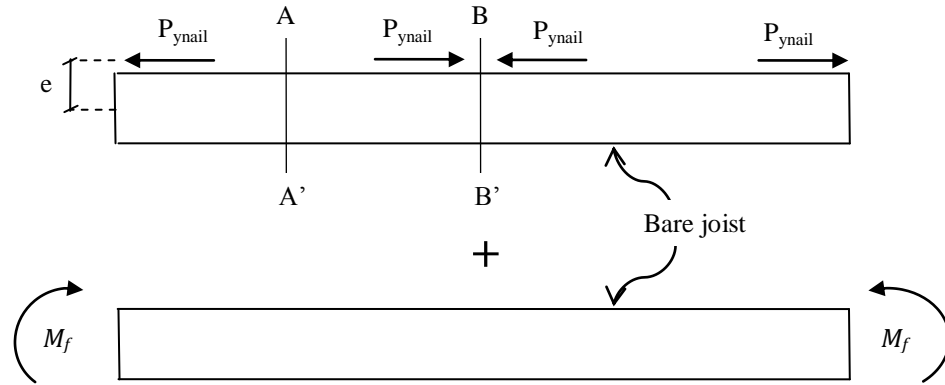
Figure 4.19 Superposition of forces acting on the joist.

As shown in Fig. 4.19, if section A-A' is considered, the end nail causes a moment opposite to those caused by the external loading, generating compression stress at the bottom of the joist as shown in Fig. 4.20 (a).
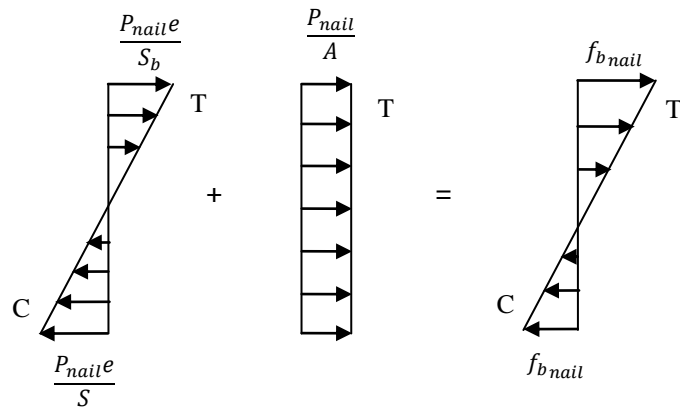
(a) Stress in joist due to nail forces only.
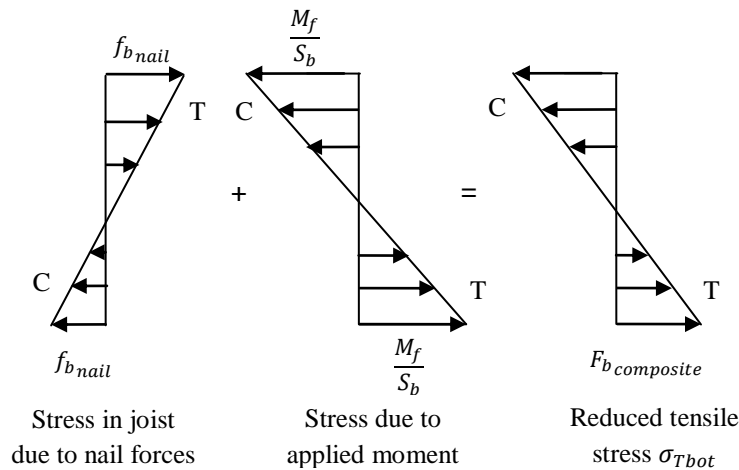
(b) Overall normal stress in joist.

Figure 4.20 Joist stress distribution due to nail forces.

51

When superimposing these conditions, a tensile stress reduction is obtained at the bottom of the joist at section A-A' as shown in Fig. 4.20 (b). This tensile stress at the bottom of the joist, σ_{Tbot}, is given by

$$\sigma_{Tbot} = \frac{M_f}{S_{bare}} + f_{b_{nail}}, \tag{4.5}$$

where

M_f is the applied external bending moment,

S_{bare} is the section modulus of the bare joist,

$$f_{b_{nail}} = \frac{P_{y_{nail}}}{A_{bare}} - \frac{P_{y_{nail}}e}{S_{bare}}, \tag{4.6}$$

P_{ynail} is the force carried by the nail after yielding,

e is the moment arm, and

A_{bare} is the bare joist cross-sectional area.

Note that Eq. (4.5) is similar in form to Eq. (2.14) from the analysis of Rosowsky and Yu [Rosowsky and Yu 2004], with the difference that Eq. (4.5) considers the yield strength of the nails, while Eq. (2.14) assumes a linear behavior of the nails.

According to classical Euler-Bernoulli beam theory, this reduction in stress would be lost at the location of the gap (section B-B') because of the equal and opposite forces of the nails, meaning that the stresses at that section would be those from a bare joist analysis. Nonetheless, an FEA of the two cases shown in Fig. 4.19 was also performed. If only the bare joist is analyzed with applied constant concentrated forces at the location of the edge nails, the axial normal stress distribution for a distance between the nails, d_{nail}, equal to 2" is obtained from the FEA at the location of the gap, and is shown in Fig. 4.21(b).

52

Location of the
gap

d_{nail}

P_{vnail} P_{ynail} P_{vnail} P_{vnail}

Joist

(a)

P_{ynail} P_{ynail}

(b)
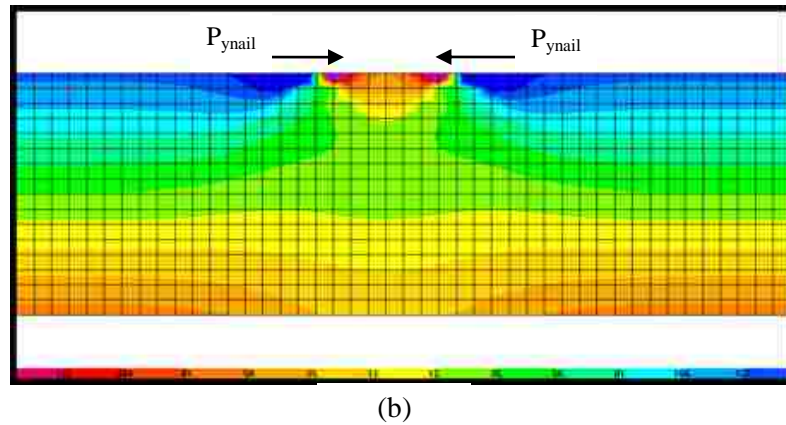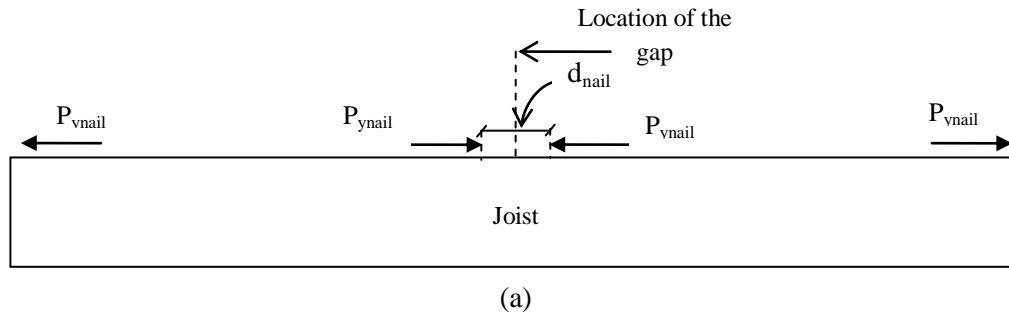
Figure 4.21 Local effects due to concentrated force acting on the joist.

The stress distribution at the location of the gap is shown in Fig. 4.22.

Stress distribution at section at the location of the gap

Joist Height (in)

Normal Stress (psi)
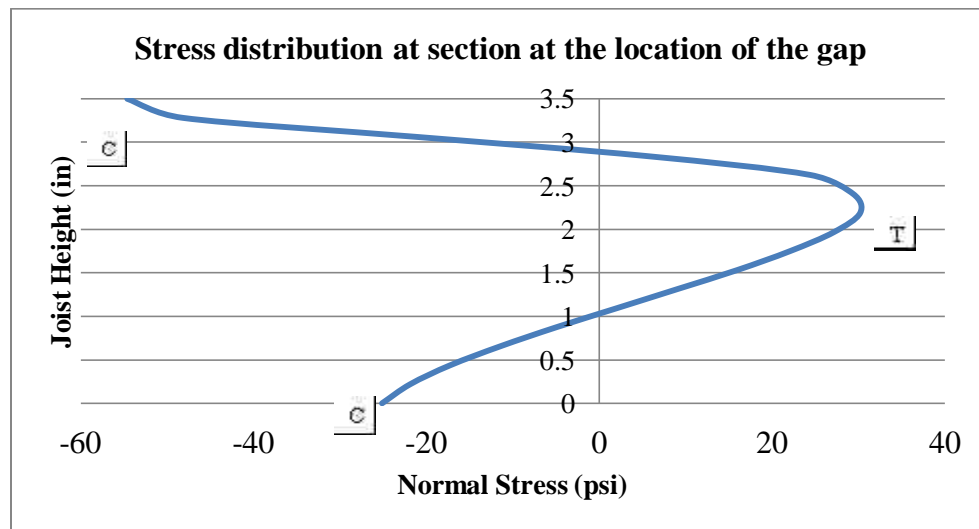
Figure 4.22 Stress distribution at the location of the gap due to local effect of nails when $d_{nail} = 2$".

When the condition of the bare joist with concentrated forces applied at the location of the end nails is superimposed with the condition of a joist under constant

53

moment at the supports, the results given by the FEA in Fig. 4.21 and 4.22 show that even at the location of a gap, the tensile stress at the bottom of the joist will have a lower value than that in a bare joist due to local effects of the nails, which generate a small compression stress at the bottom of the joist. The reduction in stresses at the location of the gap can be explained by Saint-Venant's principle, where the basic assumptions of the Euler-Bernoulli beam theory approach are no longer valid near concentrated forces and plane sections do not remain plane after deformation if the section in consideration is closer than a certain distance to the location of the concentrated force. This effect is shown in Fig. 4.23, where the compressive stress developed at the location of the gap was plotted as a function of the position of the nail forces (d_{nail}).

Compressive stress at location of gap due to nail forces
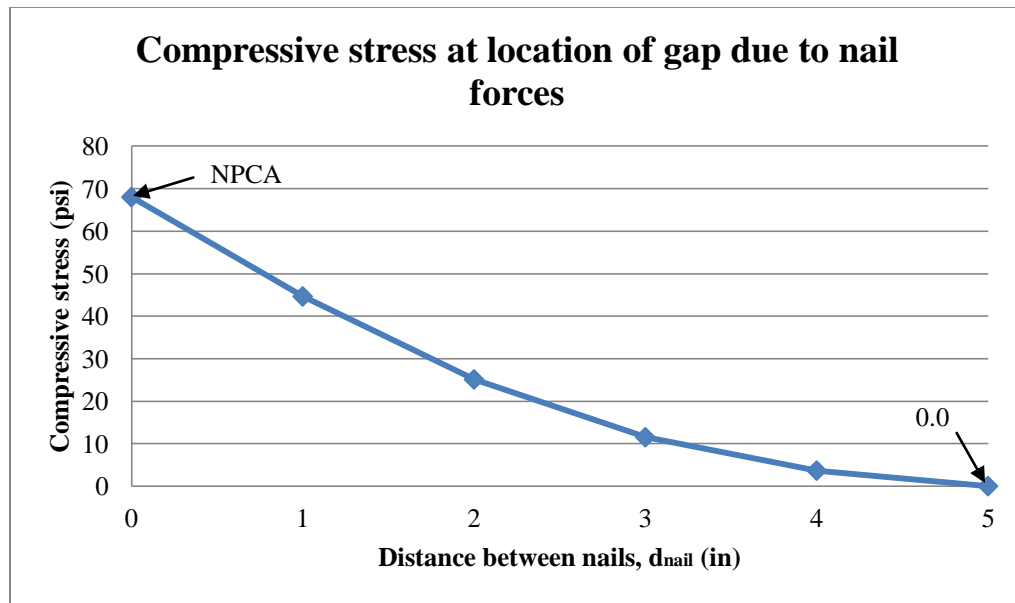
Figure 4.23 Local effects of nails on stress at the bottom of the joist.

Thus, even when gap discontinuities in the top flange are present, there is going to be a slight decrease of the tensile stress acting at the bottom of the joist. Considering the case when d_{nail} is equal to 2", and modifying Eq. (4.5), Eq. (4.7) is obtained:

$$\sigma_{Tbot} = \frac{M_{tot}}{S_{bare}} + f_{b\,nail_{gap}}, \qquad (4.7)$$

where

$fb_{nailgap} = -25.122\ psi$ (from finite element analysis for $P_{ynail} = 175$ lb).

54

These local effects are illustrated in Fig. 4.24 showing a comparison between the stress distribution obtained from the finite element analysis and the bare joist solution. Also the reduction in tensile stresses given by Eq. (4.5), at sections located away from the gaps can be observed.
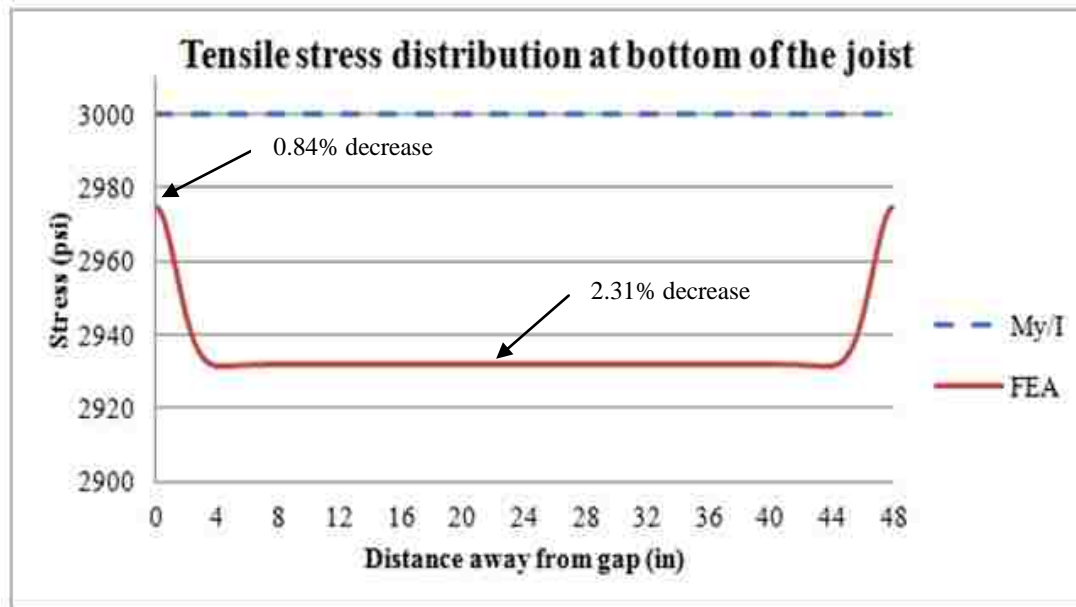
Figure 4.24 Tensile stress distribution at the bottom of the joist.

4.6 Conclusions

Although it has been shown that NPCA slightly reduces the tensile stresses at the bottom of the joist at sections away from the gap discontinuity in the flange, the overall strength of the joist is barely increased, because at the location of the gap NPCA is not longer taking any effect and the tensile stresses are only reduced by the local effects of the nails. However, these local effects are small and the contribution of NPCA can be negligible if no other parameters like the size and location of knots along the span are taken into consideration.

The next chapter takes into account these parameters in a statistical analysis and proposes a statistical increase in strength due to NPCA.

55

Chapter 5   Statistical Analysis

5.1 Introduction

Because of the small increase in strength that the results of the analytical analysis showed in Chapter 4, a Monte Carlo simulation is utilized to assess the statistical increase in strength of visually stress graded joists due to the contribution of the OSB sheathing with at least one gap discontinuity. The basic assumption for this simulation is that the wood joist will fail at the location of a knot, which has a lower bending strength (as the effective cross section of the joist is reduced by the size of the knot), and that the joist will have a higher bending strength at sections with no defects (clear wood 5% exclusion limit, given by ASTM Standard D2555 [ASTM International 2005]). This lower strength at the knots can be increased when the knots are located at a certain distance away from the location of the gap, where the tensile stresses are lowered by the NPCA. Also, based on the FEA, this lower strength at the knots can also be increased (but by a smaller percentage) in the case where the knot is close to or right underneath the location of the gap.

5.2 Simulation parameters and description

It is important to note that many parameters can be varied randomly in this simulation to achieve a more accurate and realistic increase in the strength of the joist. Some of these parameters are: external loading conditions, position of the gap with respect to the length of the joist (the gap will not always be exactly at midspan), and the bending strength of the joist as a function of the size, shape, and location of the knots, as is described in ASTM D245 [ASTM International 2005] along the span of the joist. However, in this simulation, the only random variable that is utilized is the location of the closest knot with respect to the position of a gap in the flange of the T-beam, in order to demonstrate the idea simply.

The knots considered in the simulation are assumed to be edge knots in the wide face, at the bottom of the joist (knots under maximum tensile stresses). The knots are assumed to be evenly spaced along the span of the joist. All transverse sections with a

knot are assumed to have the same strength ratio (defined in ASTM D245 [ASTM International 2005] as the ratio of moment-carrying capacity of a member with cross section reduced by the largest knot to the moment carrying-capacity of the member without defect, as shown in Fig. 5.1), ψ_{knot}, obtained from Table 4 from the same ASTM standard for an specific maximum knot size.
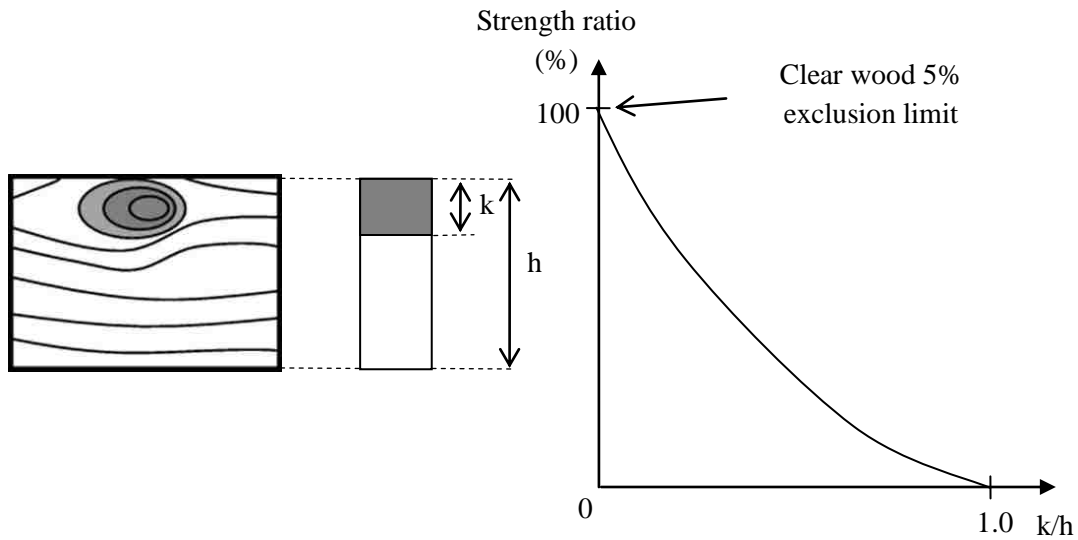
Figure 5.1 Strength ratio of the joist as a function of the knot size. Figures obtained from the Wood Handbook [Forest Products Laboratory 2010].

The statistical variation in strength (if the joist is only subjected to a constant external moment at each end), will be a function of the distance of the closest knot with respect to the location of a gap (varied with a random uniform distribution), d_{knot}, as shown in Fig. 5.2.
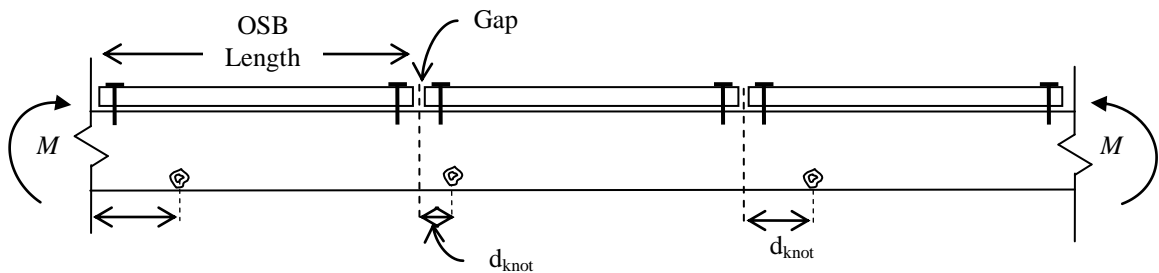
Figure 5.2 Knot position with respect to the gap in the flange.

ال管ارة للاستشارات

The simulation evaluates each position of a knot (given by d_{knot}), and checks three possible conditions for the locations of the knots in the joist in each iteration. The first condition is when a knot is located in the lowered stress region (lower bound condition, section A-A' from Fig. 4.18). The nominal moment that can be applied to the section is obtained from solving Eq. (4.5) for M_n, and substituting the tensile bottom stress, σ_{Tbot}, by the bending strength of the bare joist at the location of a knot, F_{bknot} (given by Eq. (5.1)), resulting in Eq. (5.2):

$$F_{b_{knot}} = F_b * \psi_{knot} \tag{5.1}$$

$$M_n = S_{bare}(F_{b_{knot}} - f_{b_{nail}}) \tag{5.2}$$

where

M_n is the maximum nominal moment that can be applied when knots are in the constant stress region produced by NPCA (away from gaps), and

S_{bare} is the section modulus of the bare joist.

Similarly, the second condition is present when a knot is located near or beneath to the position of a gap (upper bound condition, section B-B' from Fig. 4.18). Modifying Eq. (4.7), Eq. (5.3) is obtained (beneath a gap):

$$M_{n_{gap}} = S_{bare}(F_{b_{knot}} - f_{b_{nail_{gap}}}) \tag{5.3}$$

where

M_{ngap} is the maximum nominal moment that can be applied to the T-beam if a knot is located below a gap, and

$fb_{nailgap}$ is equal to *-25.122 psi* (from FEA for $P_{ynail} = 175$ lb).

For simplicity, at sections near the location of the gap, linear interpolation between the lower and the upper bound conditions is utilized to obtain the magnitude of

58

the maximum nominal moment of the joist in lieu of the exact stress distribution given by the FEA. As shown in the analysis, the stress tends to increase at the proximities of the gap; the starting section where the tensile stress begins to increase is approximated by adding or subtracting one height of the joist to the location of the gap, as shown in Fig. 5.3.
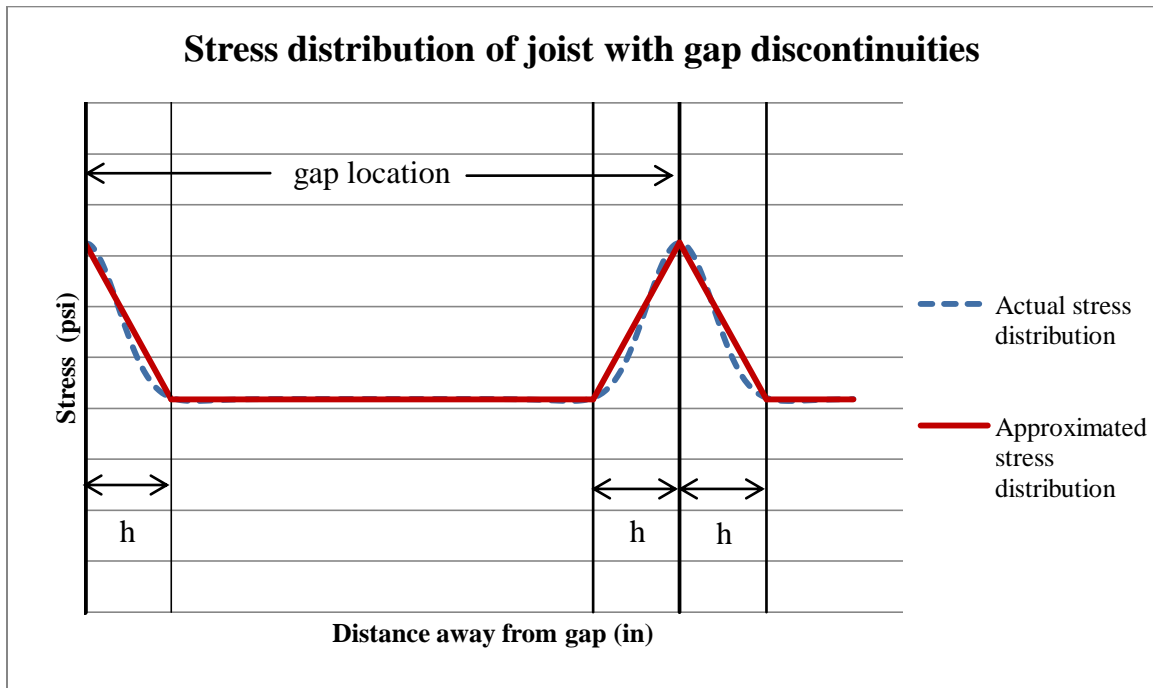
Figure 5.3 Tensile stress distribution utilized in Monte Carlo simulation.

The final condition is when all the knots are in the lowered-stress region (no knots near the location of the gap), and NPCA increases F_{bknot} to a strength greater than the bending strength of the clear wood (5% exclusion limit), F_b. Thus, the nominal moment that can be applied to the T-beam will be controlled by F_b at the location of the gap. This condition also applies if there are no knots in the joist (clear wood). Modifying Eq. (4.7) by substituting F_{bknot}, by F_b, Eq. (5.4) is obtained:

$$M_{n_{gap}} = S(F_b - f_{b_{nail_{gap}}})$$ (5.4)

59

In conclusion, the nominal moments for the three possible conditions, are compared and the minimum of them is selected and stored to be plotted in the final frequency-strength distribution.

5.3 Simulation

A MATLAB code was developed to perform the Monte Carlo simulation (shown in Appendix A). A simple example is developed next to illustrate the use of this simulation and to explain the statistical variations obtained from its results.

5.3.1 Example No. 1

The following parameters were utilized:

Number of samples: 100,000,

number of bins (for the frequency-strength plot) = 1000

concentrated constant force, P_{ynail}, = 175 lb at each end nail,

knot spacing = 24 in,

OSB panel length = 24 in,

number of gaps in the joist = 1 (for half a joist as shown in Fig. 5.4),

5% Exclusion limit for clear wood, considering White Fir = 4293 psi (obtained from Table 1 ASTM Standard D2555 [ASTM International 2005], and

strength ratio = 67% (Permitted strength ratio for select structural grade, which allows a maximum size of knots of ¾" in the joist, according to Table 7-2 in the Wood Handbook [Forest Products Laboratory 2010] and to Table 4 in ASTM D245 [ASTM International, 2005]).

These parameters satisfy the condition that the minimum bending strength of the joist (either F_{bknot} or F_b) has to be greater than 2500 psi so that the nails are able to yield and develop the 175 lb.

60
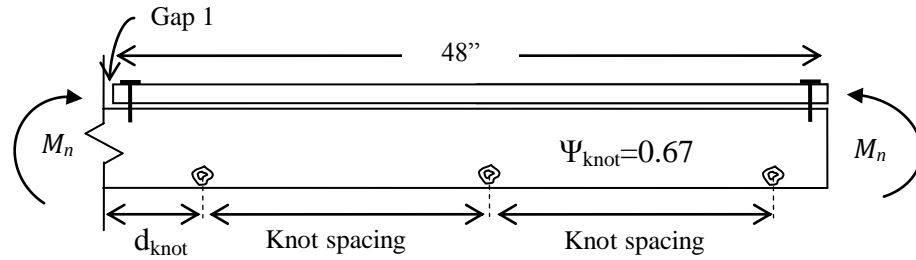
Figure 5.4 Wood joist considered in Monte Carlo simulation for Example No. 1.

The following results were obtained:
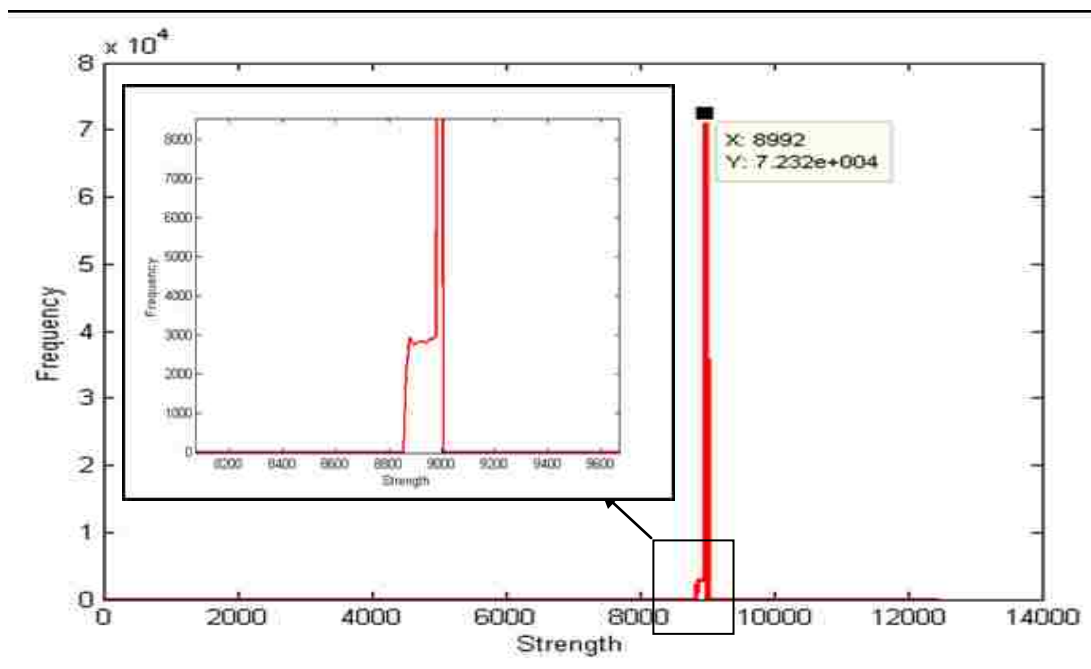
Figure 5.5 Frequency vs Strength distribution.

The two bending strengths of the joist at the limits shown in Fig. 5.4 can be easily calculated by Eqs. (5.2, 5.3 and 5.4), giving the values of:

M_n = 9010.8 lb-in (upper value, calculated from Eq. (5.2)), and

M_{ngap} = 8883.6 lb-in (lower value, calculated from Eq. (5.3)).

As shown in Fig. 5.5, most of the trials yielded a value of M_n (first condition) because most of the knots are in the lowered-stress region produced by NPCA and only

61

in the cases where a knot happened to be in the limits of the linear interpolation (or at the gap location), the nominal moment M_{ngap} controlled (second condition), hence, showing a small variation next to the peak in frequency-strength distribution.

Also, the third condition, $M_{ngap} = 13221$ lb-in, calculated from Eq. (5.4) never controlled because of the large difference in assumed strengths. If a higher strength ratio is utilized, then this calculation may start controlling in some instances.

The behavior of the frequency strength distribution shown in Fig. 5.5 can be confirmed because with the provided knot spacing in this example, the maximum distance that a knot can be away from a gap is 12 inches, which means that the strength will have a variation only if one of the evaluated knots is in the interpolation region (3.5 inches from the gap), meaning that probabilities of $3.5/12 = 29.16\%$ of having a knot in that region and 70.84% of having it in the constant stress region should be obtained. These values can be verified in Fig. 5.5 where the frequency for the strength for this case is around 72.32%, but approaches the 70.84% value as the number of specified bins increases. The mean strength value is 8992.3 lb-in, with a standard deviation of 35.022 lb-in. The strength of a bare joist is given by:

$$M = F_{b_{knot}} S$$

For this example:

$$M = 4292 \, psi(0.67)(3.0625 in^3) = 8806.65 \, lb - in$$

When comparing the strength of the bare joist with respect to the mean strength of the T-beam, a statistical increase of 2.11% is given; and when comparing it to the lower bound value of the statistical increase in strength (worst case scenario of having a knot at the location of a gap), the increase is 0.87%. This confirms that even in the worst case when a knot is located at the location of the gap there will be a small increase in the strength of a joist due to the OSB sheathing.

5.4 Analysis of the results

It is important to note that as the strength ratio allowed in each stress grade category increases, the relative effect of the NPCA will decrease because f_{bnail} remains constant due to nail yielding. At the same time, as the strength ratio decreases (lower grade joists) then the effect of the NPCA is higher and a higher statistical increase in bending strength can be obtained.
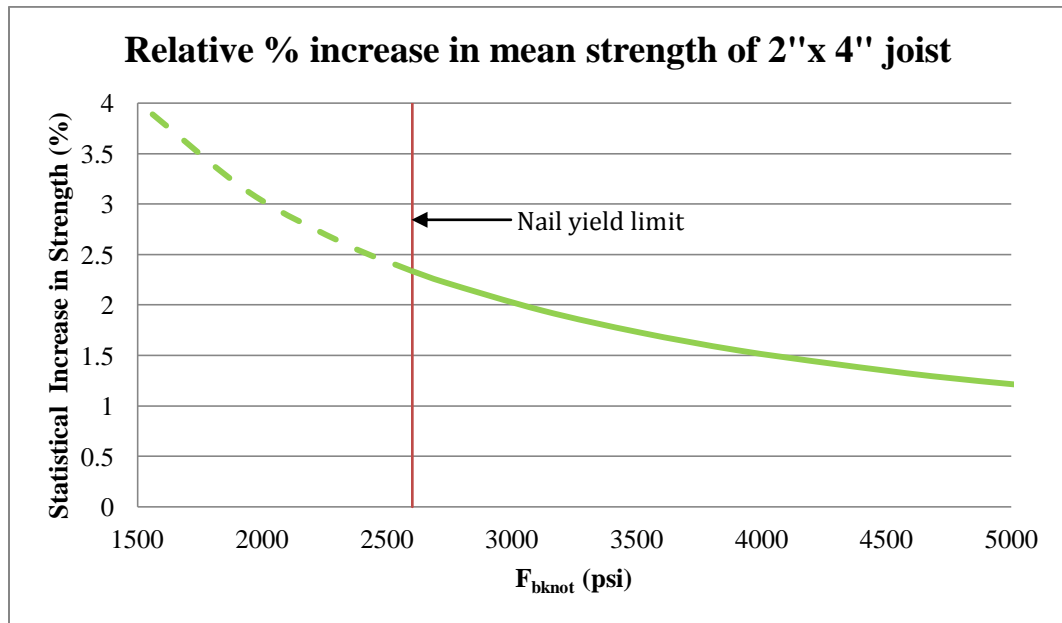
Figure 5.6 Relative increase in mean strength of 2"x 4" joist due to NPCA.

This effect of the joist mean strength is shown in Fig. 5.6, where the Monte Carlo simulation was utilized to obtain the statistical increase in strength (using the mean strength) for different bending strengths of bare joists by using the same parameters from example No. 1. Also plotted in this figure, is the minimum value of the joist strength to yield the nails.

As already mentioned, another parameter that directly affects the statistical increase in a given joist is its strength ratio. If the strength ratio is low, then it means that the knots are big and that failure of the joists will be controlled by the bending strength at the location of the weakest knot, F_{bknot}. If the structural grade of the joist is higher (as shown in Fig. 5.7 and Table 5.1), then the size of the knots will have more limitations and

the strength ratio will increase. If the case of clear wood is considered (strength ratio of 100%, given by ASTM Standard D2555 [ASTM International 2005]), then the statistical increase is very small and is given only because of the reduction of stresses at the bottom of the joist due to local effects of the nails.
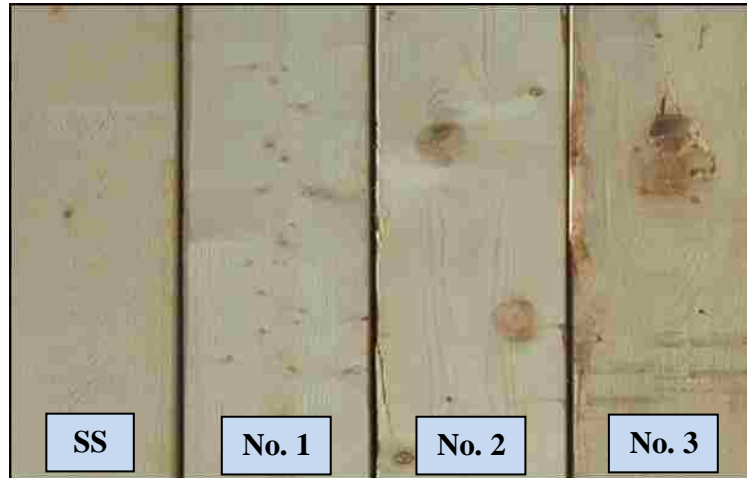
Figure 5.7 Size of knots in visually graded dimension lumber. Image obtained from Structural Building Components Association [SBCA 2009].

Structural Grade	Knot limitation
Select Structural (SS) $\Psi = 0.67$	Sound, firm, encased and pith knots are to be tight, well spaced and limited up to 7/8". Unsound or loose knots or holes are limited up to ¾", one per 4' lineal.
No. 1 $\Psi = 0.55$	Knots must be of same type as in Select Structural grade, up to 1-1/2". Unsound or loose knots or holes are limited up to 1", one per 3' lineal. Wane is allowable.
No. 2 $\Psi = 0.45$	Well-spaced knots of any quality up to 2", with one hole up to 1-1/4" per 2' lineal. Wane and skips are included.
No. 3 $\Psi = 0.26$	Knots of any quality can be up to 2-1/2", with one hole up to 1-3/4" per foot. Wane and skips are included.

Table 5.1 Knot limitation for visually graded dimension lumber [SBCA 2009].

64

Fig. 5.8 shows the relative increase in strength as a function of the strength ratio allowed per structural grade. As shown in this figure, increases of up to 9.32% in the mean strength of the joist are predicted by the Monte Carlo simulation, although in order to reach these increases, high values of the 5% exclusion limit for bending strength of the wood species in consideration (given by ASTM Standard D2555) would be needed so that the nails can start yielding before joist failure.
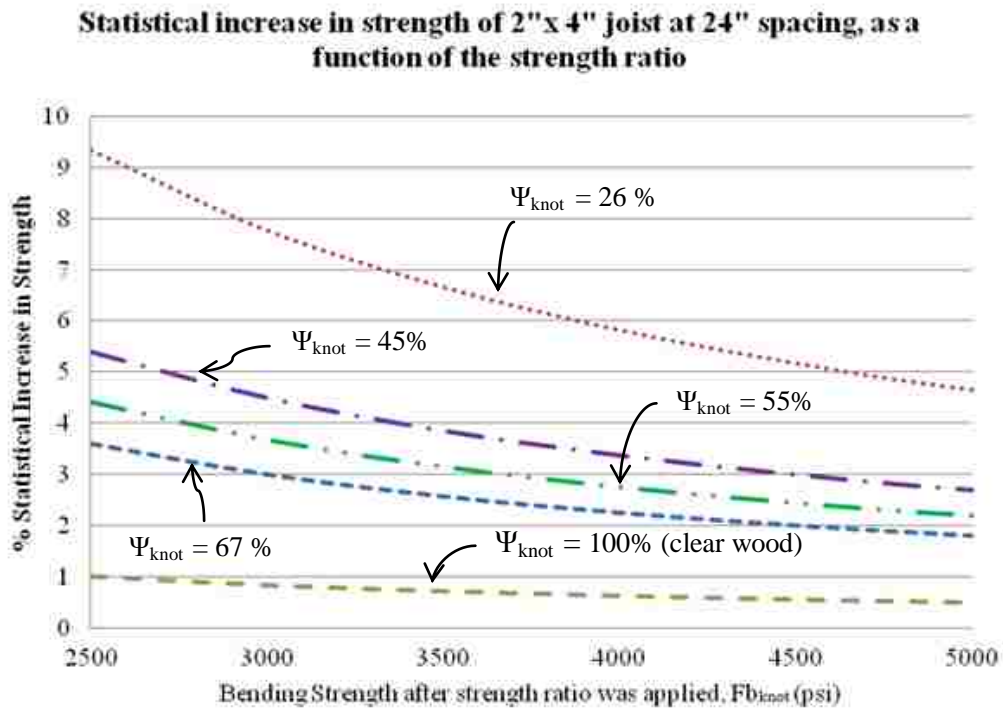
Figure 5.8 Statistical increase in strength as a function of the strength ratio.

5.5 Conclusions

The mean strength of the joist is shown to be increased, at least statistically, due to the effects of NPCA by utilizing a Monte Carlo simulation. This increase varies as a function of the structural grade and the magnitude of the bending strength 5% exclusion limit of clear wood. If more random variables are used in the simulation, then the increase in strength might be somewhat higher.

65

A useful variable that might affect this increase would be the strength ratio. Current practice assumes that the largest knot that is measured controls the strength ratio of the whole joist, which is utilized to obtain its allowable or ultimate bending strength. In reality, not all the knots will be of the same size, meaning that different sections throughout the joist will have different strength ratios. As said earlier, the chance of having a knot right beneath the gap is small, and the chance of having the largest knot in the joist at the location of the gap is even smaller. Thus, the effects of NPCA might predict a bigger statistical increase in strength than what the current analysis shows. The high variability that the bending strength of clear wood has (95% of the joists have a higher bending strength than the 5% exclusion limit), along with the random location and size of knots with respect to the location of the gap would explain the actual behavior of the T-beams in the laboratory experiments, where a significant increase in the bending strength was observed.

Chapter 6   Retrofitting Roof Assemblies

6.1 Introduction

As mentioned in Chapter 5, a way to justify an increase in the mean bending strength of wood joists under constant moment due to NPCA has been shown. However, this increase is small and the problem of carrying the extra load from the PV modules still needs to be solved. In this chapter, a few possible retrofitting techniques are proposed as well as topics for future research and development.

6.2 Structural failures

Wood structures can have various failure behaviors, which can range from splits in the members due to moisture content changes and shrinkage, to catastrophic failures and total building collapse due to excessive loads. A description of some of the most common causes of structural failure of wood framing systems that are not related to special events like fire and hurricanes follows.

Failures are often caused by incorrect sizing of the principal load carrying members for minimum design loads given by local codes, failure in connections (like in plate-connector trusses, mechanical fasteners, etc.), structural instability due to buckling or lateral torsional buckling (inadequate bracing), and bad maintenance and treatment of members (like constant moisture content changes and decay, as they may affect the structural properties of the wood).

A study of several structural wood failures in residential buildings due to a severe snow storm (which was registered in a two-week period in the Spokane/Coeur d'Alene area) was performed by the Structural Engineers Association of Washington (SEAW) [SEAW, 2009]. The study showed that the snow loads acting on the roof framing systems due to the storm were still lower than the minimum design loads specified in the local code, meaning that properly designed and constructed structures should have been able to resist this loading. However, 57 wood structures failed in this period. Out of these 57 structures, 23% failed due to bending. Several joists from the framing systems appeared

67

to have failed due to a single weak point (at a knot or split). The other 77% failed in different members or at connections (42% plate connector trusses, 26% heavy timber trusses with purlins, and 9% others).

The majority of the wood beam and joist framing systems that failed were low-slope roofs (which are susceptible to drainage and ponding issues), most having slopes of ¼" per foot or less. These flat roofs constituted 47% of the structural failures.

Figure 6.1 Snow sliding. From study of structural failures associated with the winter 2008-2009 snow event in the Spokane/Coeur d'Alene area [SEAW, 2009].

Also this study showed that older houses were more susceptible to failure than new houses. This was attributed to the improved design provisions for snow drifting, sliding, and unbalanced loading in recent building codes. The study also mentions that defects such as knots become more brittle when subjected to seasonal moisture and thermal cycles.

Failures in the wood structures varied from minor failures (excessive deflections or members that were able to be repaired) to partial building collapse. Out of the 57 failed wood structures, only one roof was totally collapsed and one was partially collapsed (around 1/5 of the total roof). All of the other structures presented failures that were repairable, as only one or two joists failed in zones where a localized accumulation of snow occurred, as shown in Fig. 6.1. This failure behavior is an important consideration,

68

as the loads apparently were redistributed to other joists with higher strength by two-way action and/or load-sharing effects, avoiding catastrophic failures.

Apparently, if unballasted PV panels are put on a retrofitted roof that has satisfied the strength requirements for this extra load, and the roof were to fail due to excessive snow loads, it is unlikely that the failure would be sudden, catastrophic, or unsafe.

6.3 Limiting considerations for retrofitting techniques

A few limiting considerations (due to efficiency and economical reasons) need to be taken into account when proposing a possible retrofit to the roof joists of existing residential houses to satisfy the strength requirements of added PV modules.

Often, there is limited space to work in the areas where the retrofits are needed. Big retrofits like adding new supports or joists to the framing system to redistribute the PV modules loads would take a lot of time and would be difficult to perform. Also, there is limited access to the exterior side of the sheathing due to roofing materials (shingles, insulation layers, etc.). If these materials are removed, then the cost of a possible retrofit would increase. Therefore, these retrofits need to be relatively easy to perform in confined spaces, must be generic enough to apply to different framing systems (while satisfying certain specifications and conditions) without requiring a structural engineer to analyze each particular retrofit, and finally, they need to satisfy their final purpose of shortening the time of the engineering certification process for the installation of the PV modules.

6.4 Retrofitting techniques

6.4.1 Provide continuity to the structural sheathing

As it was shown in Fig. 4.24, the bending strength of a joist is increased due to NPCA by only a few percent because of the gap discontinuity in the flange, as the tensile stresses at this location are almost those from a bare joist analysis and only a statistical increase was demonstrated by using a Monte Carlo simulation. Hence, a first method of a

69

possible retrofit for roof joists that need a higher strength is to provide continuity to these gaps between OSB panels. This flange continuity would be achieved by cutting pieces of OSB of 1' x 2' approximately (free space between joists) and gluing them at the locations of intermediate gaps (where no blocking or perpendicular beams are located), as shown in Figs. 6.2 and 6.3.
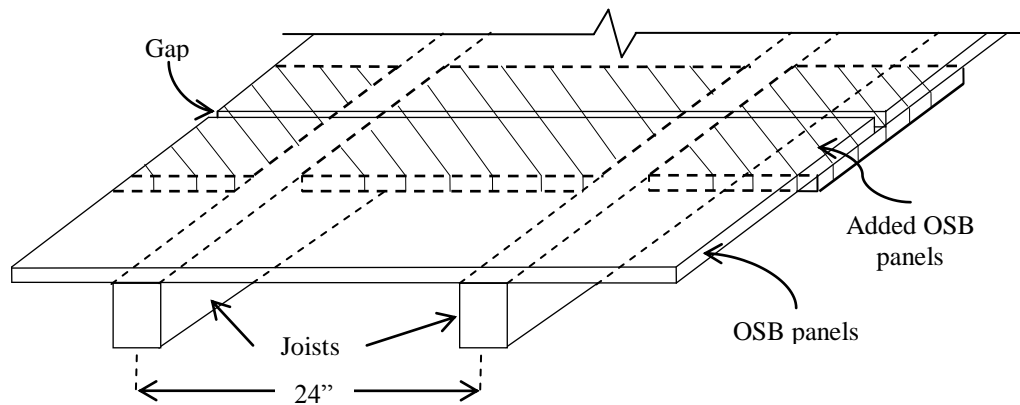
Figure 6.2 Schematic of added panels.
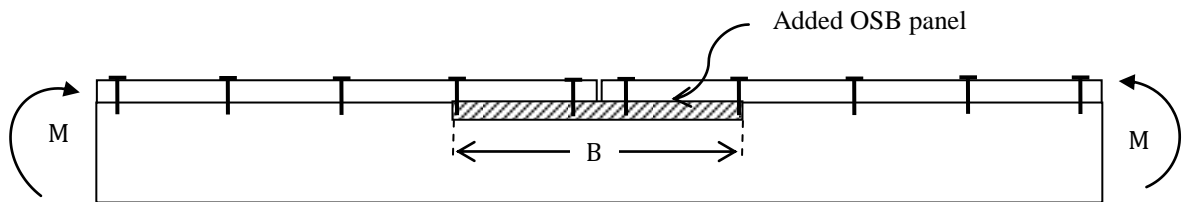
Figure 6.3 Side view of T-beam with continuous flange.

If the wood joist has a continuous flange, then the bending tensile stresses at the bottom of the joist can be calculated by using the approach developed by Rosowsky and Yu [Rosowsky and Yu 2004] if the behavior is LPCA. However, for failure loads, this method no longer applies and NPCA will control. If NPCA is controlling, then the same approach as in Section 4.4 can be utilized and the complete length of the continuous OSB panel can be considered for the calculation of the interlayer slip of the nails given by Eq. (4.4) to obtain the nail forces acting on the flange according to their load-displacement curve. With this higher length, more nails would yield when the failure moment is reached (not only the end nails as assumed in Chapter 4), as shown in Fig. 6.4, and hence,

70

more nails can be considered in the analysis of NPCA to achieve a higher bending strength of the joist.
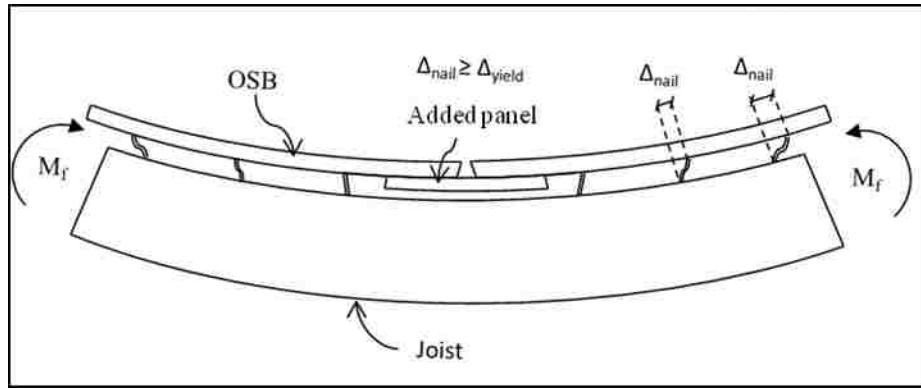
Figure 6.4 Deformation of the nails.

Fig. 6.5 shows a free-body diagram of the forces acting on the joist due to the nails. Fig. 6.6 also shows the shear forces the glue in the added panel would have to carry. The width B of the panel would be obtained as a function of the needed length of glue at the interface.
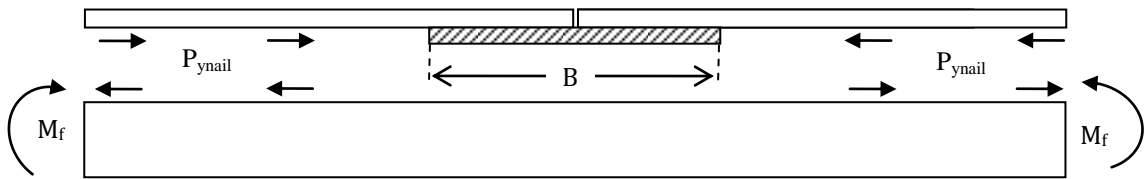
Figure 6.5 Free-body diagram of the nail forces acting at the joist.

Figure 6.6 Free-body diagram of forces acting at the flange and at the added panel to provide continuity.

A Monte Carlo simulation can still be utilized to achieve a higher increase the strength of the T-beam subjected to constant moment even when continuity is provided to the flange, because the random location of knots in the joist would still play a key role. In

this case, the critical location of the knots is not determined with respect to the position of a gap (as considered in Chapter 5 with the discontinuous flange); instead, the critical location would be determined with respect to the position of the yielding nails. If more nails are considered by NPCA, sections close to midspan would have the lowest tensile stress, although this tensile stress would increase after the location of each nail towards the end of the joist (where the strength of the joist at a knot may start to control failure). Nevertheless, this condition would be important only for a joist subjected to constant moment whereas in more common loading conditions (as three-point bending or distributed load), the maximum bending moment in the joist will be located at midspan, while the less stressed regions are located near the supports.

In addition to the continuity of the flange, if two strips of glue are put on the sides of the joist as shown in Fig. 6.7, an even higher increase of the bending strength might be reached, as a higher shear force would be transferred into the flange. In this way, the flange would take a higher percentage of the total moment, and the T-beam would reach full composite action (FCA). If a simple analysis considering full composite action is performed to the same T-beam used in the analysis of Sections 4.3 and 4.4, then the width, w, needed to resist the shear force at the interface would be only of approximately ½" on each side of the joist.
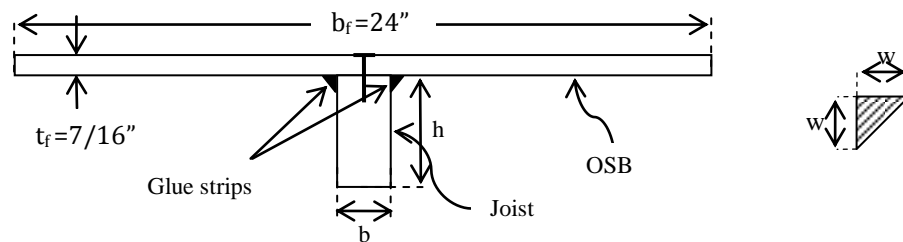
Figure 6.7 Added glue strips at each side of the joist.

Nevertheless, there are some aspects to consider if the gaps in the sheathing panels are removed, some of these are: linear expansion of the OSB panels due to changes in moisture content or temperature could cause compressive stresses in the flange because of the constrained deformation that the continuity would provide. This

effect may even cause buckling in the OSB, Also, the procedure for gluing the pieces of OSB to the flange needs to be specified.

6.4.2. Reinforcing the joist at the location of the gap

This retrofitting technique proposes to reinforce the region near to the location of the gap so that the T-beam can resist the increased bottom tensile stresses at this location. A first method of reinforcing this region is to increase the area of the joist by attaching two sister joists at each side of the T-beam as shown in Fig. 6.8. These two sister joists should be of the same height of the roof joists, with a width, b', to be determined by the necessary area increase and with a length of 2h (plus some development length to be determined in tests), based in Fig. 4.24 and shown again in Fig. 6.9. The procedure of gluing the two sister joists in an effective way would be a topic of future research, as well as the effects of variable moments of inertia along the span of the T-beam.
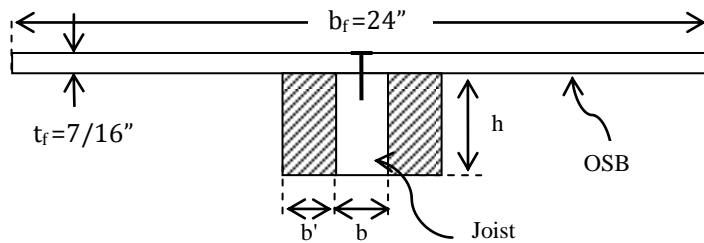
Figure 6.8 Increased transverse section of T-beam.

Tensile stress increase at location of a gap
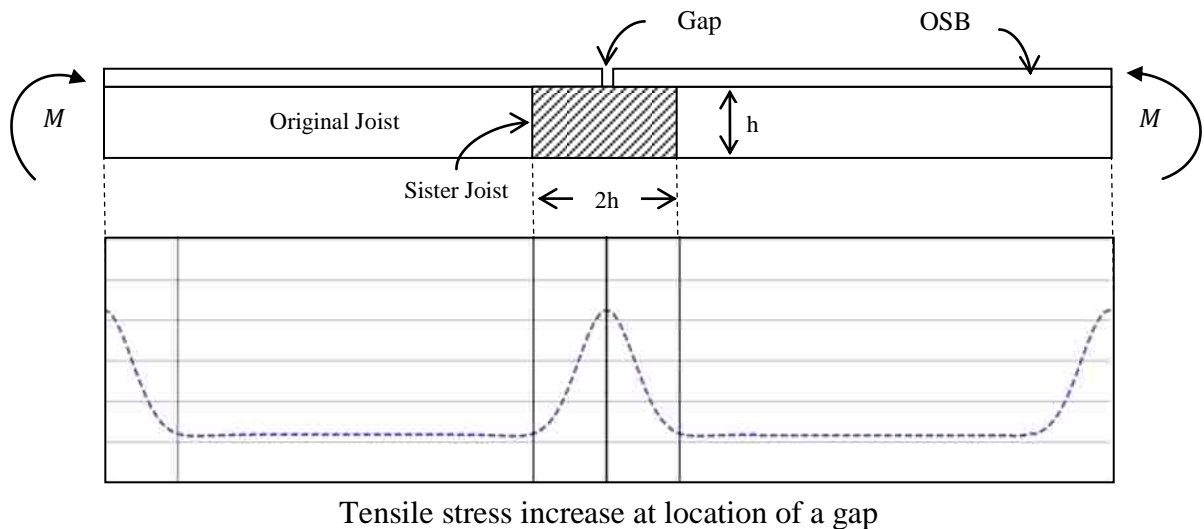
Figure 6.9 Side view of reinforcement of the T-beam at the location of the gap.

73

A second possible method of reinforcing the region with higher tensile stresses would be to screw and glue a thin steel plate (with prebored holes) as shown in Fig. 6.10. The thickness of the plate can be obtained by assuming full composite action in this region. The effects of doing this reinforcement to the joist (like different moments of inertia and different locations of the neutral axis in the same member) need to be considered.
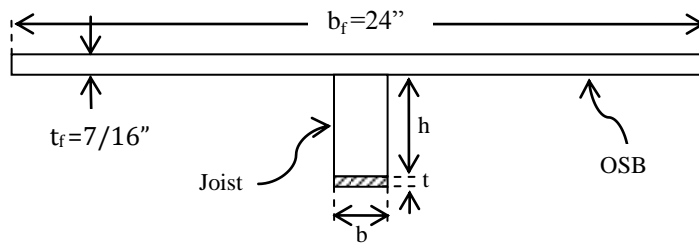
Figure 6.10 Thin plate at bottom of the joist.
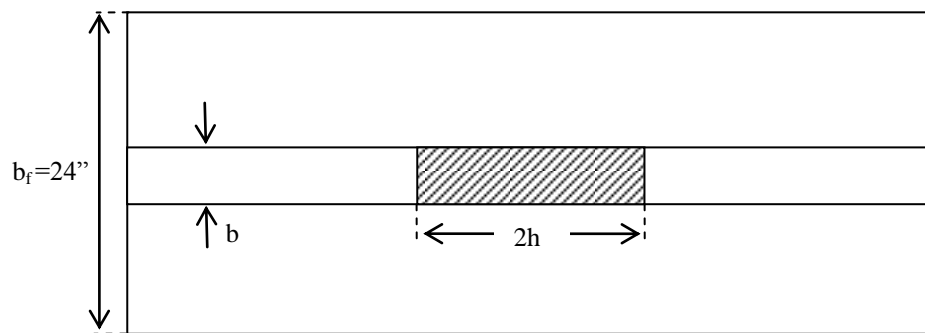
Figure 6.11 Plan view of thin plate at bottom of the joist.

6.5 Conclusions

Generic, easy to install and effective procedures of retrofitting roof joists considering and enhancing the beneficial effects of NPCA were proposed to account for the loads from the PV modules. If research is continued in this topic, greater increases in the bending strength of the joists might be reached, hence helping the solar industry to further develop.

74

Chapter 7   Summary and Conclusions

7.1 Summary

The structural considerations that represent a market barrier to the installation of PV modules were studied. The need for existing roof framing systems to resist the extra load of the PV modules lead to the proposed methods to resist these loads without having to conduct expensive retrofits that might delay or even cancel PV module installation. One of these possible methods to justify an increased strength is to consider composite action between wood joists and the structural sheathing attached to them. A simple model that can be easily utilized by practicing engineers to justify an increase in the bending strength of visually stress graded joists was proposed for one loading condition.

Although the NDS design code recognizes system effects in the 15% increase to the allowable bending strength of the joist due to load sharing only, it was believed that composite action needed to be reconsidered, because in previous simple models (not computer based models), the gaps in the sheathing were not taken into account in any strength calculation and the interface was assumed to behave linear elastically.

Several laboratory experiments were performed, where the flexural strength of visually stress graded 2"x 4" bare wood joists (different structural grades were utilized) was compared to the strength of joists with a layer of OSB sheathing attached with nails. This assembly forms a composite "T-beam" with the OSB panel being the flange and the wood joist being the web. Gaps between the OSB panels were considered in the bending strength of the T-beam. Also direct-shear tests were performed to obtain the mechanical properties of nailed and glued-and-nailed connections. Tests results showed that even with the gap discontinuity, the T-beams were significantly stronger than the bare joists, and that failure at the wood joists initiated at the location of a weak knot, rather than at the location of the gap as it was expected (where the highest tensile stresses are located). This behavior was confirmed by the fact that some T-beams with glued-and-nailed connections failed at lower loads than the nailed-only connections, leading to the hypothesis that failure of the joist is a function of the location of the weakest knot with respect to the location of the gaps. Therefore the bending strength of joist can be

75

increased at least statistically, as the chance of having a weak knot at the location of a gap is small.

Detailed theoretical and numerical analyses of this composite section were also performed. Two limiting cases were considered to estimate the magnitude of the nail forces being transferred between the joist and the flange. In the first limiting case, the behavior was assumed to be fully composite, while in the second limiting case, the flange and joist were both assumed to be axially infinitely stiff, and the connection infinitely soft. Both limiting cases showed that the nail-wood connection has a nonlinear behavior when failure loads are applied to the T-beam, hence developing NPCA. However, the load-displacement curve of the nailed connection and the small forces that the nails can transfer to the flange, make the second limiting case closer to the actual behavior of the T-beam.

The theoretical analysis also showed that NPCA (where only the two yielded nails at the end of each OSB panel are conservatively considered to be the only nails transferring force) decreases the bottom tensile stresses of the wood joists at sections away from the location of the gap. At the location of the gap, the basic mechanics of materials approach predicts that the NPCA would be lost, and that the tensile stresses at the bottom of the joist would be those from a bare joist analysis. However, the numerical analysis showed that the tensile stresses at the location of the gap still are slightly reduced due to Saint-Venant's principle. Thus if the location of the weakest knot in the joist is far from the gap discontinuity, then NPCA will decrease the tensile stresses acting on it and hence, increase the overall bending strength of the T-beam. However, if a weak knot is near the location of a gap, then the tensile stresses will almost be those from a bare joist analysis and only a small increase in strength due to composite action is obtained.

A statistical model was developed, using a Monte Carlo simulation to randomly vary the location of the knots (weak points in the joist), and based on the strength ratio and the bending strength 5% exclusion limit of clear wood, a small statistical increase in the mean bending strength of the joist and its standard variation were obtained. However,

76

this increase is a function of the bending strength of the bare joist and its structural grade, as the size and location of the knots have more limitations for higher grade joists.

Finally, an analysis of the behavior of the structural failures of wood structures was studied. In the case the statistical increase in strength of the joist due to NPCA is not enough to account for the extra weight given by the PV modules, some retrofitting techniques were proposed to strengthen the joists based on the analyses and the results of this research.

7.2 Conclusions

As it was observed in the results of the laboratory experiments, there is a clear increase in the bending strength of the wood joists due to the attached OSB panels, even when using a non-rigid connection like a nailed joint, and a discontinuous flange due to gaps in the structural sheathing. This behavior was observed in all of the tests, although a high variation in the bending strengths of the tested joists was obtained due to the variability in the bending properties of wood, but still in each case, the bending strength of the T-beam was always significantly higher than that of a bare joist.

The theoretical analysis showed that forces in the nails are in their nonlinear region when failure loads are applied to the composite T-beam and according to the load-displacement curve of the nailed connection, NPCA is developed in the joist. However, the forces that the nails are able to carry are small and hence, the flange is resisting only a small percentage of the total moment acting on the T-beam.

A glued-and-nailed connection between the wood joist and the structural sheathing was found to be stronger, as higher shear force would be transferred to the flange (although the location of the knots with respect to the location of the gap still needs to be considered), but it is not a very practical retrofit for existing roof structures.

All the analyses performed in this thesis are for the condition of constant moment throughout the length of the joist, which is the worst case scenario for nail yielding and

77

might be a starting point for further research where other loading conditions can be considered.

The statistical simulation (where the knot location was varied) showed an increase in the mean bending strength of the joists. However, these statistical increases are small and depend on the allowed strength ratio and on the bending strength 5% exclusion limit for clear wood for the species in consideration.

For higher grade joists like No. 1 or select structural (where the location and size of knots have greater limitations, meaning high strength ratios), the effect of NPCA decreases and only small bending strength increases are achieved. However, for lower grade joists (as for No. 3 joists or studs, with low strength ratios, and typically used in wall systems) the effect of NPCA increases and higher increases in the bending strength of the joists are achieved (up to 9%, as shown in Fig. 5.8), because bigger knots are allowed, and hence, NPCA will reduce the tensile stress acting on them. Nonetheless, according to Eq. (4.4) and Fig. 4.16, there is a minimum 5% exclusion limit value that the wood species in consideration needs to satisfy in order to guarantee that the end nails yield and produce NPCA when failure moment is reached.

However, these predictions of strength increase are small and do not match the increases observed in the laboratory experiments (60% average increase in Sections 3.2 and 3.3, and 22% average increase in Section 3.5) where the number of laboratory tests might have been insufficient to produce a statistically significant data set. The high variability that the bending strength of clear wood has (95% of the joists have a higher bending strength than the 5% exclusion limit), along with the random location and size of knots with respect to the location of the gap might be possible explanations of the behavior of the laboratory experiments.

If not only the location of the knot is used as a random variable in the Monte Carlo simulation, and more variables are used (like size of the knot, loading conditions, location of the gap, etc) then a higher statistical increase in the mean strength should be obtained. Current joist grading practices, assume the largest knot that is measured to

78

determine the strength ratio utilized to obtain the allowable properties of the joist. However, not all the knots are of the same size and different sections throughout the length of the joist have different strength ratios. Hence, the chance of having the biggest knot in the joist at the location of the gap is even smaller than having any knot at that location (as considered in Chapter 5), and consequently, the effects of NPCA might give a bigger statistical increase in strength.

If the spacing of the nails is reduced at the ends of the joist, then more nails can be considered to be yielding and can be brought to the analysis of NPCA, and thus a greater increase in the bending strength of the joist could be obtained.

According to the analyses performed in this research, the NPCA effect would be lower for bigger joists (i.e. 2"x 6" or 2"x 8"), because even though the nail forces will have a larger moment arm, the effect of the gap in the OSB panels would also be larger (equal to 2h, according to Fig. 5.3), reducing the "lowered stress region" and increasing the chance of having a weak knot in that region.

Three efficient retrofitting techniques were proposed as a result of this investigation and need to be analyzed and studied for future use. If positive results are obtained, this could benefit greatly the industry of solar energy as more PV modules would be able to be installed on existing roof systems in a faster manner and at a lower cost, motivating more people to install PV modules on their roofs.

7.3 Future research

If a more accurate method to calculate the interlayer slip acting on the nails is developed, then more nails can be brought into the analysis depending on their behavior (linear or nonlinear), and a higher increase in the strength of a joist might be reached.

Different loading conditions need to be considered in the analysis of NPCA (like three-point bending or distributed load).

79

Further development of the retrofitting techniques proposed in Chapter 6, for the cases where the small increase obtained by statistical means is not enough to resist the panel loads, should be pursued.

Load sharing effects of the joist-sheathing assembly, considering the particular loading conditions of PV modules, where according to their typical distribution, only every other joist in the roof system might be loaded under four-point bending. Also, the two-way action effect provided by the stiffness of the racking system of the PV modules, together with the adjacent joists and sheathing might increase the strength of the roof.

Appendix A – Monte Carlo Simulation Matlab Code

A-1. Example No. 1

```matlab
function Example_1
clc
clear
grid on
% Monte Carlo Simulation for a 2in x 4in x 96in wood joists, with two
7/16"
%OSB panels and two nails per panel, with constant moment, varying only
the
%knot spacing randomly.
% Input number of samples required in the study.
nsamples = 100000;
% Bin size
num_bins = 1000;
% Input dimensions of the joist.
width = 1.5;
height = 3.5;
strength_ratio = 0.67;
number_gaps = 1;
% Input parameters for gaps and knots.
OSB_length = 24;
knot_spacing = 24;
Length_joist = OSB_length*number_gaps;
number_knots = Length_joist/knot_spacing;
% Properties of the section.
c = height/2 ;
I = width*height^3/12 ;
S = I/c;
A = width*height;
% Effective bending strength at any location without a knot.
Fb_rup = 4292; % 5% EL for clear wood (obtained from ASTM D2555).
% Effective bending strength at knot location.
Fb_rup_knot = Fb_rup*strength_ratio;
% Nail data.
F_nail = 175;
fb_nail = F_nail/A - F_nail*height/(2*S);
fb_nail_gap = -25.122; %from FEA (local effects).
constant_moment = (Fb_rup_knot-fb_nail)*S; % lb-in
moment_gap_knot = (Fb_rup_knot-fb_nail_gap)*S; % lb-in
% Set limits and ranges.
Mn_range_max = 1.4*moment_gap_knot;
Mn_range = [0 : Mn_range_max/num_bins : Mn_range_max-
Mn_range_max/num_bins];
frequency = zeros(1, num_bins);
Mn = zeros(nsamples,1);
% Start varying the location of the knots and evaluate the nominal
bending
% moment of the section.
knots = zeros(1,number_knots);
gap_position = zeros(1,number_gaps);
% Gap position:
for i = 1 : number_gaps
    gap_position(i) = (i-1)*OSB_length;
```

```matlab
    end
    % Calculate relative position of the knots
    for i = 1 : number_knots
        knots(1,i) = (i-1)*knot_spacing;
    end
    Mn_knot = zeros(number_gaps,number_knots);
    for m = 1 : nsamples
        knot_position = knots + knot_spacing/2*rand;
        % Check all knots with respect to gap position.
        for i = 1:number_gaps
            for j = 1 : number_knots
                if (gap_position(1,i) <= knot_position(1,j)) &&
(knot_position(1,j) <= gap_position(1,i) + height)
                    Mn_knot(i,j) = constant_moment + (moment_gap_knot -
constant_moment)*(height + gap_position(1,i) -
knot_position(1,j))/height;
                elseif (knot_position(1,j) > gap_position(1,i) - height) &&
(knot_position(1,j) < gap_position(1,i))
                    Mn_knot(i,j) = constant_moment + (moment_gap_knot -
constant_moment)*(knot_position(1,j)-(gap_position(1,i)-
height))/height;
                else
                    Mn_knot(i,j) = constant_moment;
                end
            end
        end
        controlling_Mn_knot = min(Mn_knot(:));
        % Check if the section at midspan is controlling:
        moment_gap = (Fb_rup - fb_nail_gap)*S;
        controlling_moment = min(moment_gap,controlling_Mn_knot);
        Mn(m) = controlling_moment;
        % Get the frequency of each value and assign it to an interval.
        ibin = floor(num_bins*Mn(m)/Mn_range_max);
        frequency(ibin) = frequency(ibin) + 1;
    end

    % Plot of Strength vs Trial
    % figure;
    % plot (Mn, '-rs', 'LineWidth',2,'markerfacecolor','b',...
    %        'markeredgecolor', 'none','markersize',1);
    % xlabel('trial');
    % ylabel('strength');

    plot (Mn_range, frequency, '-rs',
'LineWidth',2,'markerfacecolor','b',...
        'markeredgecolor', 'none','markersize',1);
    xlabel('Strength');
    ylabel('Frequency');

    Mn_mean = mean(Mn)
    Mn_std_dev = std(Mn)

end
```

References

ANSI/AF&PA NDS-2005 National Design Specification (NDS), for Wood Construction with Commentary and Supplement.

American Forest & Paper Association (AF&PA) (2005). National Design Specification for Wood Construction. American Forest & Paper Association, Inc.

American Society of Civil Engineers (ASCE) (2010). Minimum Design Loads for Buildings and Other Structures ASCE/SEI 7-10.

ASTM Standard D2555-06 (2011). "Standard Practice for Establishing Clear Wood Strength Values" ASTM International West Conshohocken, PA, 2003, DOI: 10.1520/C0033-03A, www.astm.org.

ASTM Standard D245-00 (2002). "Establishing Structural Grades and Related Allowable Properties for Visually Graded Lumber" ASTM International West Conshohocken, PA, 2003, DOI: 10.1520/C0033-03A, www.astm.org.

ASTM Standard D3498-03 (2011). "Standard Specification for Adhesives for Field-Gluing Plywood to Lumber Framing for Floor Systems" ASTM International West Conshohocken, PA, 2003, DOI: 10.1520/C0033-03A, www.astm.org.

Aune, Petter; Patton-Mallory, Marcia, (1986). "Lateral load-bearing capacity of nailed joints based on the yield theory: Theoretical development". Res. Pap. FPL 469. Madison, WI. U.S. Department of Agriculture, Forest Service, Forest Products Laboratory.

Cramer, S. M., Drozdek, J. M., and Wolfe, R. W. (2000). "Load sharing effects in light-frame wood-truss assemblies." J. Struct. Eng., ASCE 126(12), 1388–1394.

Cramer, S. M., and Wolfe, R. W. (1989) "Load-distribution model for light-frame wood roof assemblies." J. Struct. Eng., ASCE, 2602– 2616.

Douglas, B.K. and Line, P., (1996). "System Effects in Wood Assemblies", Proceedings of the International Wood Engineering Conference, New Orleans, LA.

Forest Products Laboratory. (2010). Wood handbook—Wood as an engineering material. General Technical Report FPL-GTR-190. Madison, WI: U.S. Department of Agriculture, Forest Service, Forest Products Laboratory. 508 p.

Foschi, R. O. "Structural analysis of wood floor systems" (1982). J. Structural Div., ASCE, 108(7), 1557-1574.

Gupta, R., Miller, T.H. and Dung, D. (2004). "Practical Solutions to Wood Truss Assembly Design Problems. Practice Periodical of Structural Design and Construction", 9(1), pp. 54-60.

Kuenzi, E. W., and Wilkinson, T. L. (1971). "Composite Beams—Effect of Adhesive or Fastener Rigidity", Research Paper FPL 152, Forest Products Laboratory, USDA, Forest Service, Madison, Wis.

Limkatanyoo P. (2004). System Behavior of Three-Dimensional Wood Truss Assemblies. MS thesis, Oregon State University, Corvallis, OR, USA.

Liu, W. F., and Bulleit, W. M., (1995). "Overload Behavior of Sheathed Lumber Systems" J.Struc. Eng., ASCE, Vol. 121(7), 1110-1118.

McCutcheon, W. J. (1977). Method for predicting the stiffness of wood-joist floor systems with partial composite action. Res. Pap. FPL 289. Madison, WI: USDA, Forest Service, Forest Products Laboratory.

McCutcheon, W. J. (1986). Stiffness of framing members with partial composite action. J. Struct. Eng., ASCE, 112(7), 1623-1637.

84

McCutcheon, W.J. (1984). "Deflection of uniformly loaded floors: A beam-spring analog" USDA Research Paper FPL 449, Forest Products Lab., Madison, Wis.

McLain, T. E. (1975). "Curvilinear load-slip relations in laterally loaded nailed joints", Ph.D. dissertation, Colorado State University, Fort Collins, CO, USA.

Mi, H. (2004). "Behavior of unblocked wood shearwalls". MScFE thesis. University of New Brunswick, Fredericton, NB.

Mohammad, M. A. H. & I. Smith (1994). "Stiffness of nailed OSB-to-lumber connections". Forest Products Journal, 44, 37-44.

National Association of Home Builders (NAHB), (2000). "Residential Structural Design Guide: 2000 Edition", Washington, DC.

Pellicane, P. J., Stone, J. L., Vanderbilt, M. D. (1991). "Generalized Model for Lateral Load Slip of Nailed Joints". J. Mater. Civ. Eng., Vol. 3, No. 1.

Polensek, A. (1976). "Finite element analysis of wood-stud walls". J. Structural Div., ASCE, 102(ST7): 1317-1335.

Rancourt, D. G. (2008). "Structural Behavior of Wood I-Joist/OSB Roof Panel Assemblies" MS thesis, University of Maine, Orono, Maine, USA.

Rosowsky, D. V., and Yu, G. R. (2004). "Partial factor approach to repetitive-member system factors." J. Struct. Eng., ASCE, 130(11), 1829-1841.

Structural Building Components Association (2009) "Truss Technology in Building: Lumber Grades".

Structural Engineers Association of Washington (SEAW), (2009). "Study of Structural Failures Associated with the Winter 2008-2009 Snow Event in the Spokane/Coeur d'Alene Area.

Thompson, E. G., Vanderbilt, M. D., Goodman, J. R. (1982). "FEAFLO: A program for the analysis of layered wood systems". Computers and Structures VII: 237-248.

Wang, Q. (2009). "Relationship between fastening properties and load-deflection response of wood shear walls", MScFE thesis. University of New Brunswick, Fredericton, NB.

Wei-Feng Liu, and Bulleit, W.M. (1995). "Overload behavior of sheathed lumber systems". J. Struct. Eng., ASCE, 121(7), 1110–1118.

Wheat, D. L., Vanderbilt, M. D., and Goodman, J. R. (1983) "Wood floors with nonlinear nail stiffness." J. Struct. Eng., ASCE, 109(5), 1290-1302.

Wilkinson T. L. (1972). "Analysis of nailed joints with dissimilar members" J. Structural Div. Amer, Soc. Civil Eng. Vol. 98, No. ST9 p. 2005-2013. Proc. Pap. 9189.

Wilkinson T. L. (1974). "Elastic bearing constants for sheathing materials" USDA For. Serv. Res. Pap. FPL 224. For. Prod. Lab. Madison, Wis.

Wolfe, R. W. (1990). "Performance of light-frame redundant assemblies." Proc., 1990 Int. Timber Engineering Conf., 1, 124–131.

Wolfe, R. W., and LaBissoniere, T. (1991). "Structural performance of light-frame roof assemblies. II. Conventional truss assemblies". Research Paper FPL-RP-499, U.S. Dept. of Agriculture, Madison, Wis.

Wolfe, R. W., and McCarthy, M. (1989). ''Structural performance of light-frame roof assemblies. I: Truss assemblies designed for high variability and wood failure.'' Research Paper FPL-RP-492, U.S. Dept. of Agriculture, Madison, Wis.

Yu, G. (2003). "Load sharing and system factors for light-frame wall systems." PhD dissertation, Oregon State University, Corvallis, Oregon.